S
uis

FACULTY OF SCIENCE AND TECHNOLOGY

MASTER'S THESIS

Engineering structures and Materials / Mechanical Engineering	Spring, 2023 Open
Author: Sangmin Park	
Supervisor at UiS: Knut Erik Teigen Giljarhus	
Thesis title: Wind tunnel CFD simulation by using openfoam	
Credits (ECTS): 30	
Keywords: Openfoam, wind tunnel, CFD, support interference, wall interference, drag coefficient	Pages: 44 Stavanger, *8th June, 2023*

Abstract

Aerodynamics and fluid dynamics are used in many fields, such as aerospace, marine, and oil & gas. All these industries require precise results from experiments, tests, and simulations. This is because it is connected to considerable risks and losses. However, getting a perfectly correct answer in a fluid dynamic world is impossible. So, an approximation is used to solve unsolvable equations. This led people to simulate and test with CFD and wind tunnels. A wind tunnel is a test machine to test the fluid flow over the minimized object and expect how it will be in the real world. To test it in the real world, the size of the product is too huge and very expensive. Therefore, wind tunnel testing is essential.

This dissertation it was verifying CFD conducted processes by using Openfoam for the new wind tunnel at Universitetet i Stavanger. First, the log law of the wall was verified. This process was confirmed without any model inside the wind tunnel. After this verification, grid optimization and wall distance effect were done to reduce errors and check for any corrections. Pressure distribution, velocity distribution, and drag coefficient were used as criterion properties to check any difference in each case. The mesh size did not have any significant effect on the results. However, the wall distance affected the results because of the wall interference. Finally, support interference was carried out. Support interference is also one of the significant factors that can affect the result, as well as wall interference. These interferences are the most significant differences between the natural world and the wind tunnel. The existence of the supports behind the test model interrupted the vortex creation. Also boundary layer along the supports affected the pressure distribution. All these factors influenced the drag coefficient of the disk model. As a result, the drag coefficient decreased by 3%. This is because of the location of the supports. The supports must locate far away from the model so it does not affect the vortex formation.

Table of Contents

List of Figures

List of Tables

1 Introduction

Seven mathematical problems have not been solved yet. People call it "Millennium Problems." One of the problems is the Navier-Stokes equation. It has more variables than equations, so it is only able to have approximate values as answers. Navier-Stokes is one of the most important equations in the fluid dynamics field. If it can have an exact solution from it, it will be able to expect all fluid-related problems, such as forecasting climate. Unfortunately, it is not possible to have an exact solution. Therefore, it is important to do many experiments and simulate some situations by using machines and computers. Luckily, nowadays, by using computational fluid dynamics (CFD) and wind tunnels, it can get approximate solutions. A wind tunnel is one of the experimental equipment to predict flow movement. This aerodynamic result can be utilized and applied to many different fields. Since it can give very reasonable solutions, many industries researched this. However, some industry fields, such as oil and gas and aviation industries, require more detailed and precise results because some errors can occur economic loss. In the worst case, they can bring about loss of lives. In the case of a wind tunnel, it is a machine that researchers can observe what is happening directly.

In many cases, experiments are assumed to be held in open space. However, a wind tunnel is a sort of pipe, which means it is a closed environment. This can occur some errors. Therefore, in this dissertation, by utilizing CFD, results will be simulated and compared to the actual empirical data conducted with a new wind tunnel at Universitetet i Stavanger (UiS). This is to have the first appropriate setup of the wind tunnel. First, the boundary layer was checked by comparing it with theories to check if the wind tunnel could give reasonable results. Fangquing Liu mentioned two different ways to analyze regions close to the wall. The first method is integrating the turbulence into the wall. This method requires a large number of mesh numbers. The second method is wall functions. Wall functions are defined as empirical equations satisfying the physics of the flow close to the wall. These are used to connect the inner flow region and the fully developed region (Liu, 2017). And then, a small disk is located in the middle of the wind tunnel's test section. By using OpenFOAM and Paraview, air flow movement tendency could be checked. In this dissertation, obtaining grid optimization and appropriate area ratio between the wind tunnel and the disk model is conducted. Velocity and pressure profiles were checked. Furthermore, drag profiles were obtained to get more precise and practical data. Drag and lift are the most essential properties in wind tunnel testing. The distance between the model and the wall is not very far, so they can affect each other. Ernad, Fuad, and Samir reference that a blockage correction factor is needed because of the blockage effect of the closed section of the wind tunnel (Ernad, et al., 2020). Atsushi showed that using Morky's method, it got corrected drag coefficients and showed good agreement with the result from CFD without a wall (Atsushi & Masataka, 2012). Checking drag can give a conclusion of wind tunnel testing simulation conditions to have reliable data.

At last, the support interference drag effect will be measured. Adding on to the wall blockage effect, support can affect the total drag measurement of the disk model. According to low-speed wind tunnel testing (Jewel, et al., 1997), drag to the disk generated by support often represents 10% to 50% of the minimum drag of the whole object. Drag with and without supports are also measured and compared to each (S Russo, 2020). Checking support interference is crucial to obtain more precise wind tunnel testing results. Because of the supports, the wind flow pattern changes behind the model. All these processes will be held using the OpenFOAM program's CFD simulation.

1.1 Wind tunnel

A wind tunnel is a machine that can measure how fluid moves along or over an object. We can check the change in wind velocity and properties of an object and can check what happens. By using a smoke generator, it is more visible, and it is able to observe intuitively. There are sensors in the test section so we can check drag, lift, and other force details to the object and support. By using a miniature model of an actual model, such as aircraft, we can estimate flow behaviors and prevent some accidents that can be generated by flow behavior. However, a wind tunnel is not an open space, and it generates internal flow instead of external flow. The wind tunnel is focused on conducting experiments similar environment to nature, primary research and those used in the field of aerodynamics has some limitations, such as the size of the test section, the speed of airflow, and the level of turbulence intensity in the undisturbed stream (Centrum Techniki Okrętowej S.A., 2023). Even though there are many limitations, it is still a very nice experimental tool for estimating flow behaviors. By using CFD and comparing it with experimental data, I will reduce errors caused by the limitations.
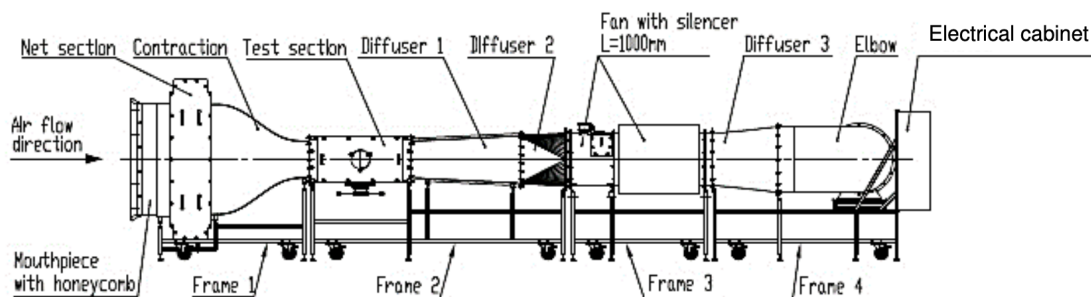
Figure 1. Presentation of the aerodynamic tunnel sections

Figure 1 is a design drawing of a new wind tunnel at UiS. It is an open circuit subsonic wind tunnel with a test section in front of the fan section. It consists of an inlet, flow straightener, honeycomb, contraction, test section, diffusers, fan, silencer, and outlet. The name of this wind tunnel is "Subsonic wind tunnel in 40 ft. container". Objects that we will observe locate in the middle of the test section, and sensors will be plugged in so that it is able to measure the properties of the objects and inside the

test section. It is allowed to change the orientation of the objects by turning the grips below the test section. It is able to have a wind velocity of 0 ~ 40m/s. The internal dimension of the test section is 1250x450x450mm.

2 Theory

2.1 Reynold's number.

Reynolds number is a fundamental dimensionless parameter for all viscosity behaviors of Newtonian fluids. It is expressed as Re.

$$Re = \frac{\rho V L}{\mu} = \frac{V L}{\nu}$$

In this equation, ρ = density, V = flow velocity, L = characteristic length, and μ = dynamic viscosity. ν = kinematic viscosity, with a ratio of dynamic viscosity μ over density ρ. By using Reynolds numbers, it is able to predict the status of flows. As a fluid engineer, the first thing the engineer has to do is measure the Reynolds number. It is able to divide flow patterns into three different flows: creeping flow, laminar flow, and turbulent flow. When Reynolds number is very low, the flow can be defined as creeping flow. Honey is an example of creeping flow. In the case of the low to middle range of Reynolds number, it is classified as laminar flow. For the high Reynolds number, it is defined as turbulent flow. Flow over a flat plate, where the length between the flat edge and the start point is L, if $Re_L \approx 5 \times 10^5$ flow pattern shows the transition from laminar to turbulence. Reynolds number can differ in different cases, such as pipe flow. If it is pipe flow and fully developed flow, the diameter of pipe D is used instead of the characteristic Length L. The transition number from Laminar to turbulent is $Re_D = 2300$ (Frank, 2011).

2.2 Boundary layer

When fluid flows along a pipe or a flat plate, uniform flow speed and speed on the wall show different behavior because the fluid flowing close to the wall is affected by shear stress because of viscosity. It is able to divide into two regions; viscous region and inviscid region. The boundary layer is a layer that divides these into regions. A flow with a low Reynolds number where the viscous effect is significant and the viscous region is thick. However, viscosity does not affect turbulence flow as much as laminar flow. So the viscous region is thin.
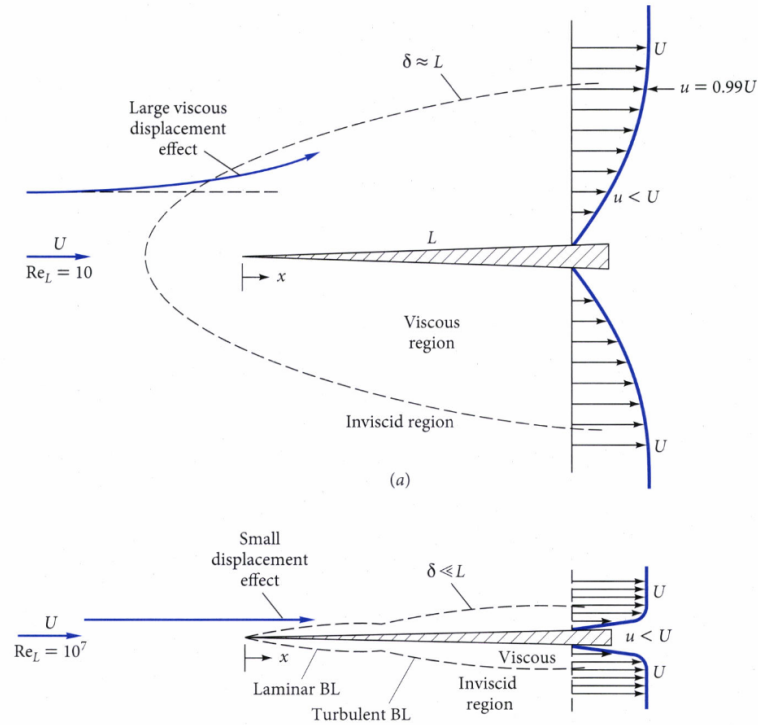
Figure 2. Boundary layer

2.2.1 Boundary layer equations

There are three methods to analyze external flows; CFD (computational fluid dynamics), experiment, and boundary layer equations. The continuity equation and Navier-stokes equation can be written below for the two-dimensional, steady state, incompressible, viscous flow, and cartesian coordinates.

$$\frac{\partial u}{\partial x} + \frac{\partial v}{\partial y} = 0$$

$$\rho \left(u\frac{\partial u}{\partial x} + v\frac{\partial u}{\partial y} \right) = -\frac{\partial P}{\partial x} + \mu(\frac{\partial^2 u}{\partial x^2} + \frac{\partial^2 u}{\partial y^2})$$

$$\rho \left(u\frac{\partial v}{\partial x} + v\frac{\partial v}{\partial y} \right) = -\frac{\partial P}{\partial y} + \mu(\frac{\partial^2 v}{\partial x^2} + \frac{\partial^2 v}{\partial y^2})$$

In 1904, Ludwig Prandtl (1875-1953) introduced boundary layer approximation. Since when Reynolds number is large boundary layer is very thin, he assumed as below.

$$Velocity: v \ (veltical \ direction) \ll u(horizontal)$$

$$Rate\ of\ change: \frac{\partial u}{\partial x} \ll \frac{\partial u}{\partial y} \quad \frac{\partial v}{\partial x} \ll \frac{\partial v}{\partial y}$$

$$Reynolds\ number: Re_x = \frac{Ux}{v} \gg 1$$

With these assumptions, it is able to simplify the continuity equation and Navier-stokes equation.

$$\frac{\partial P}{\partial y} \approx 0$$

This means that P≈P(x). In other words, pressure will be varied by only a boundary layer. Through all these assumptions, it can be able to get this conclusion.

$$\frac{\partial u}{\partial x} + \frac{\partial v}{\partial y} = 0$$

$$u\frac{\partial u}{\partial x} + v\frac{\partial u}{\partial y} \approx U\frac{dU}{dx} + \frac{1}{\rho}\frac{\partial \tau}{\partial y}$$

$$\tau = \mu\frac{\partial u}{\partial y} \quad (Laminar)$$

$$\tau = \mu\frac{\partial u}{\partial y} - \overline{\rho u'v'} \quad (Turbulent)$$

2.2.2 Boundary thickness

The boundary layer thickness δ is defined as the distance between the plate and the point where the horizontal viscous flow velocity u is the same with 99% of surface flow velocity U. Boundary layer thickness is a function of surface velocity, location, and fluid properties. The boundary thickness equation depends on the status of the flow. For laminar flow, δ is proportional to the square root of Re_x. However, this will not be applied to calculate boundary layer thickness for turbulent flow. As Re_x grows as x grows, infinitesimal disturbance in the flow begins to increase, and it will not stay as laminar flow. The transition process begins from this point, $Re_{x,critical} \cong 1 \times 10^5$ and continues until $Re_{x,transition} \cong 3 \times 10^6$.

When it comes to laminar flow, in 1908, Blausis introduced $\frac{u}{U}$ is a function of dimensionless variable η.

$$\frac{u}{U} = f'(\eta), \qquad \eta = y\sqrt{\frac{U}{\upsilon x}}$$

This ends up in the Blausis equation.

$$f''' + \frac{1}{2}ff'' = 0$$

Through this Blausis equation, it is able to calculate boundary layer thickness δ.

$$\frac{\delta}{x} = \sqrt{\frac{4.91}{Re_x}}$$

Wall shear stress τ_w is defined as the below equation.

$$\tau_w = \mu\frac{\partial u}{\partial y}\bigg|_{y=0}, \frac{d(\frac{u}{U})}{d\eta}\bigg|_{\eta=0} = f''(0) = 0.332$$

With these two equations, laminar shear stress can be obtained as below.

$$\tau_w = 0.332\frac{\rho U^2}{\sqrt{Re_x}}$$

Non-dimensionalizing wall shear stress can obtain a laminar local skin friction coefficient.

$$C_{f,x} = \frac{\tau_w}{\frac{1}{2}\rho U^2} = \frac{0.664}{\sqrt{Re_x}}$$

When it comes to turbulent flow, all the theories for laminar flow cannot be applied, and it is not able to solve the turbulent flow boundary layer equations. Therefore, all expressions about the shape and properties of the turbulent boundary layer are obtained empirically. One common empirical approximation of turbulent boundary layer is the one-seventh-power Law.

$$\frac{u}{U} \cong \left(\frac{y}{\delta}\right)^{\frac{1}{7}} \ (for \ y \leq \delta) \quad \rightarrow \quad \frac{u}{U} \cong 1 \ (for \ y > \delta)$$

This approximation cannot be very meaningful; very close to the wall because of the slope $\frac{\partial u}{\partial y}$ at y=0 will be infinite. It is able to obtain turbulent boundary layer thickness and local skin friction coefficient.

$$\frac{\delta}{x} \cong \frac{0.16}{Re_x^{1/7}}$$

$$C_{f,x} \cong \frac{0.027}{Re_x^{1/7}}$$

There are many approximation methods for turbulent boundary layers besides the one-seventh Law, such as log law, and Spalding's Law.

2.2.3   Log law

Log law is a semi-empirical expression that can be used for not only flat plate flow but also fully developed pipe flow. It consists of nondimensionalized variables by a characteristic velocity, friction velocity u_*.

$$u_* = \sqrt{\frac{\tau_w}{\rho}}$$

$$\frac{u}{u_*} = \frac{1}{\kappa} \ln \frac{y u_*}{\nu} + B \ where \ (0.4 \leq \kappa \leq 0.41 \ and \ 5.0 \leq B \leq 5.5)$$

In log law, κ and B are constants. However, the log wall does not work very well to the wall because ln 0 is undefined.

2.2.4   Spalding's Law

In 1961, D.B. Spalding created a new method that is valid all the way to the wall, and it is called Spalding's Law of the wall.

$$\frac{y u_*}{\nu} = \frac{u}{u_*} + e^{-\kappa B} \left[e^{\kappa \left(\frac{u}{u_*}\right)} - 1 - \kappa \left(\frac{u}{u_*}\right) - \frac{\left[\kappa \left(\frac{u}{u_*}\right)\right]^2}{2} - \frac{\left[\kappa \left(\frac{u}{u_*}\right)\right]^3}{6} \right]$$

14

2.2.5 u^+ vs y^+

To check the relationship between boundary layer thickness and viscous region velocity, the most common notation uses the non-dimensional variables, Law of the wall variables y^+ and u^+.

$$y^+ = \frac{yu_*}{\nu}, u^+ = \frac{u}{u_*}$$

y^+ is a type of Reynolds number. The differences among the three approximations close to the wall can be shown more clearly using u^+ and y^+ instead of using u and y.
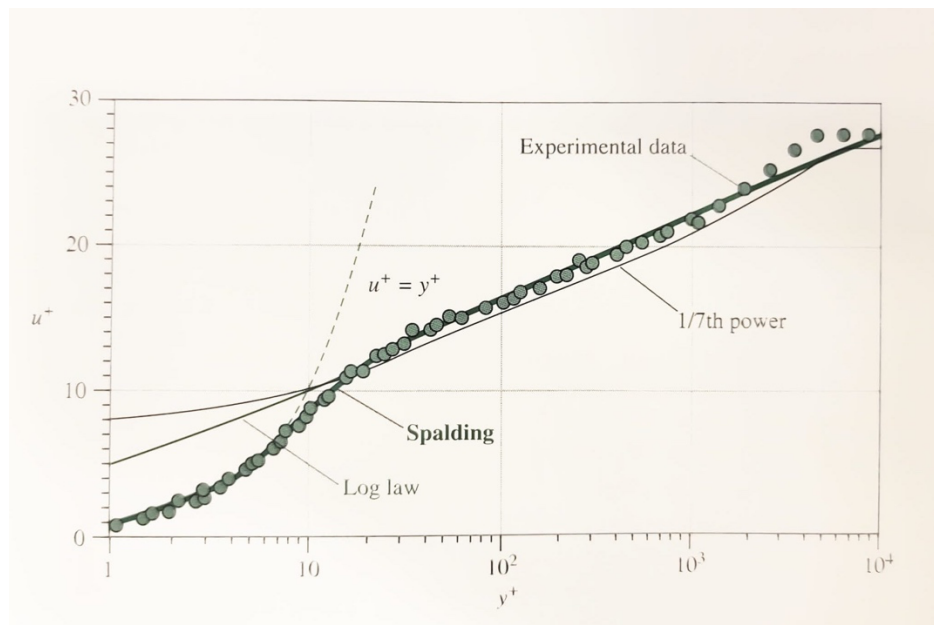
Figure 3. Comparison of turbulent flat plate boundary layer profile expressions in the Law of the wall variables at Re_x $= 1.0 \times 10^7$

(Yunus A.Çengel, 2010)

The region very close to the wall is called the viscous sublayer. It is able to see that Spalding's expression is very close to the experimental data compared to other expressions.

2.3 Aerodynamic resistance

When a fluid flows over an object, the object feels some resistance. Inside a fluid world, all moving objects feel this resistance. The force applied to the fluid movement is directed against the object, and We call this drag. The drag force is easy to measure directly by using a spring or other tools. Drag force

is a combination of pressure and wall shear forces in the flow direction. Lift is a combination of pressure and wall shear stress forces in the direction normal to the flow direction.

2.3.1 Drag

Let's say a flow is going over an object, and infinitesimal flow is moving through a differential area dA on the surface. The force from pressure is $PdA,$ and the shear force is $\tau_w dA$. The differential drag force acting on the differential area in two-dimensional flow is like below.

$$dF_D = -PdA \cos \theta + \tau_w dA \sin \theta$$

By integrating dF_D, it is able to obtain the total drag force which applies to the object.

$$F_D = \int_A dF_D = \int_A (-PdA \cos \theta + \tau_w dA \sin \theta)dA$$

In the case of a very thin flat plate aligned parallel to the flow direction, where $\theta = 90°$, the drag force occurs only by the wall shear stress. On the other hand, if the plate is aligned vertically to the flow direction, where $\theta = 0°$, the drag force occurs by only the pressure. According to (Yunus A.Çengel, 2010), it is more efficient to work with dimensionless numbers that express the drag characteristics of the body. It is a drag coefficient C_D.

$$C_D = \frac{F_D}{\frac{1}{2}\rho V^2 A}$$

A is the object's frontal area, and the project's cross-sectional area is vertical to the flow direction. The drag coefficient is a function of the shape of the body. Since we are interested in the drag for the entire surface, it is more efficient to use the average coefficient. So the average drag is able to calculate as below.

$$C_D = \frac{1}{L} \int_0^L C_{D,x}dx$$

Drag force occurs through two different independent effects, pressure and wall shear stress. Drag can be divided into skin friction drag and pressure drag.

$$C_D = C_{D,friction} + C_{D,Pressure}$$

16

Reducing skin friction drag and pressure drag is essential to reduce total drag force. However, these two drag does not decrease at the same time, and they tend to change in different ways. So it is crucial to find an optimizing way for both drags. To minimize the sum of the two different drags, the shape of the object is very important. $\frac{D}{L}$ is used to check how the shape affects total drag force, and it showed that the drag force depends on the shape of the object.

2.3.2   Drag Coefficients of common geometries

Where the Reynolds number is below 10,000, the drag coefficient usually depends on the Reynolds number. However, when the Reynolds number is over 10,000, the drag coefficient remains constant depending on the shape of the geometries. In the case of creeping flows, where the Reynolds number is below 1, the drag coefficient is inversely proportional to the Reynolds number. In the case of a circular disk, the drag coefficient is determined to be as below.

$$C_D = \frac{20.4}{Re}$$

Unfortunately, most of the situations that objects will experience is being in turbulent flows. This means Reynolds number is high ($Re > 10,000$). The orientation of the body relative to the direction of flow has a prominent influence on the drag coefficient. The drag coefficient under a high Reynolds number is nearly independent of the Reynolds number. The drag coefficient of the disk and circular rod are determined to be as below.

$$C_D = 1.1 \ (disk)$$

$$C_D = 1.2 \ (Cylinder \ Laminar)$$

$$C_D = 0.3 \ (Cylinder \ Turbulent)$$

2.4 CFD

CFD is an abbreviation of computation fluid dynamics. Before CFD, analytical fluid dynamics (AFD) and experimental fluid dynamics (EFD) were used, but due to the improvement of high-speed digital computers, CFD is available these days. CFD is a computer simulation for the prediction of fluid-flow behavior. The objective of using CFD is to model the continuous fluids with partial differential equations (PDEs) and discretize them into an algebra problem. And then, we validate it and obtain a

simulated result-based design. CFD is used to analyze and design. "Simulation-based design" is more efficient than "build and test." It is cost-effective and more rapid than doing experiments.

Moreover, data from CFD simulation provides high-fidelity data. In the case of some situations which is not easy to measure by experiment are able to measure by simulations. CFD is used in many different fields, such as aerospace, automotive, biomedical, and energy field.

2.4.1 Initial and boundary conditions

Initial conditions must not affect results, and the computer will find the convergence value that fits the equations by putting initial values. To obtain a more accurate CFD solution, boundary conditions must be applied. Basic boundary conditions are wall boundary conditions, inflow/outflow boundary conditions, miscellaneous boundary conditions, and internal boundary conditions. In the case of wall boundary conditions, the normal velocity component is set to zero since the fluid cannot pass through the wall.

Moreover, we consider a no-slip condition, so the tangential component of velocity is also zero. For the turbulence model, wall roughness must be specified. Lists of boundary conditions: no-slip or slip-free on the wall, periodic, and inlets, such as inlet velocity, mass flow rate, and constant pressure.

2.5 SST $k - \omega$ Turbulence models

The SST $k - \omega$ Turbulence model is a two-equation eddy viscosity model (CFD online, 2011). SST is an abbreviation of "Shear stress transport." This is known as a hybrid model with two different turbulence models. They are the $k - \omega$ turbulence models and the $k - \varepsilon$ turbulence models (AUTODESK, n.d.). The $k - \omega$ turbulence models applied well when the flow close to the wall needed to be simulated. This makes the SST $k - \omega$ Turbulence model very suitable to be applied as a Low Reynold's number turbulence model. The $k - \varepsilon$ turbulence model is more suitable for predicting the flow pattern away from the wall. This can prevent the model from being very sensitive to the inlet free stream turbulence properties (CFD online, 2011). By combining these two different turbulence models, it is able to apply to a simulation for both flows close to the wall and far away from the wall. The two-equation eddy viscosity model is given by the following (Langley Research Center, 2013). The transport equation for the turbulence kinetic energy is written below.

$$\frac{\partial(\rho k)}{\partial t} + \frac{\partial(\rho u_j k)}{\partial x_j} = P - \beta^* \rho \omega k + \frac{\partial[(\mu + \sigma_k \mu_t)\frac{\partial k}{\partial x_j}]}{\partial x_j}$$

The transport equation for the specific dissipation rate omega is as below.

$$\frac{\partial(\rho\omega)}{\partial t} + \frac{\partial(\rho u_j\omega)}{\partial x_j} = \frac{\gamma}{\nu_t}P - \beta\rho\omega^2 + \frac{\partial\left[(\mu + \sigma_\omega\mu_t)\frac{\partial\omega}{\partial x_j}\right]}{\partial x_j} + 2(1 - F_1)\frac{\rho\sigma_{\omega2}}{\omega}\frac{\partial k}{\partial x_j}\frac{\partial\omega}{\partial x_j}$$

All other coefficients and auxiliary relations are written below.

$$\nu_t = \frac{a_1 k}{\max(a_1\omega, SF_2)} \ (Kinematic\ Eddy\ viscosity)$$

$$F_2 = \tanh\left[\left[\max\left(\frac{2\sqrt{k}}{\beta^*\omega y}, \frac{500\nu}{y^2\omega}\right)\right]^2\right] (Second\ blending\ function)$$

$$P_k = \min\left(\tau_{ij}\frac{\partial u_i}{\partial x_j}, 10\beta^*k\omega\right) (Production\ limiter)$$

$$F_1 = \tanh\left\{\left\{min\left[\max\left(\frac{\sqrt{k}}{\beta^*\omega y}, \frac{500\nu}{y^2\omega}\right), \frac{4\sigma_{\omega2}k}{CD_{kw}y^2}\right]\right\}^4\right\} (Blending\ function)$$

$$CD_{kw} = \max\left(2\rho\sigma_{\omega2}\frac{1}{\omega}\frac{\partial k}{\partial x_i}\frac{\partial\omega}{\partial x_i}, 10^{-10}\right)$$

$$\phi = \phi_1 F_1 + \phi_2(1 - F_1)$$

The SST $k - \omega$ turbulence model combined the $k - \varepsilon$ turbulence models and the $k - \omega$ turbulence models to obtain a better prediction of wall-bounded flows.

2.6 Blockage correction

E.C. Maskell suggested a method to correct the error caused by the blockage effect for bluff bodies in the closed wind tunnel (E.C.Maskell, 1963). The method was based on momentum balance in the flow. Maskell's method is to estimate the wake blockage of the bluff bodies in closed test sections. For this method, some assumptions are necessary. The form of the pressure distribution over the bluff bodies is invariant under constraint. The separated flows show a tendency to become axially symmetric. The correction formula that Maskell suggested is the ratio between corrected dynamic pressure and obtained dynamic pressure.

$$\frac{q_c}{q} = \frac{k^2}{k_c^2} = 1 + \frac{1}{k_c^2 - 1}\frac{S}{C}$$

19

$$k^2 = 1 - C_{pb}$$

$$\epsilon = \frac{1}{k_c^2 - 1}$$

$$\frac{\Delta q}{q} = \epsilon \frac{C_D S}{C}$$

In this formula, q means dynamic pressure, S means the representative area of the model, and C means the cross-sectional area of the wind tunnel. Moreover, Δq is the effective increment in dynamic pressure because of constraint. $\frac{C_D S}{C}$ is the wake blockage parameter, and ϵ is the blockage factor. C_{pb} is the base pressure coefficient. Moreover, the "c" represents effective or corrected. To obtain the blockage factor of the bluff body, k_c^2 must be obtained. Assuming $k_c^2 = k^2$ is not sufficient to get a precise result. So the iterative solution has been found by using the formula below.

$$(k_c^2)_n = k^2 \left\{ 1 + \frac{1}{(k_c^2)_{n-1}} \frac{C_D S}{C} \right\}^{-1}$$

From all these processes, the measured value of drag and pressure coefficient can be corrected by following the formula. C_{Dc} is the corrected drag coefficient. And C_p means the pressure coefficient.

$$\frac{q_c}{q} = \frac{k^2}{k_c^2} = \frac{C_D}{C_{Dc}} = \frac{1 - C_p}{1 - C_{pc}}$$

According to Fail, Lawford, and Eyre's experiment, the square, circle, and triangular base pressure coefficient is -0.36 (R.Fail, et al., 1959). The relation between dynamic pressure and drag coefficient can be written below.

$$\frac{q_c}{q} = 1 + \epsilon C_D \frac{S}{C}$$

Maskell mentioned that the blockage factor could be replaced with the empirical constant 2.5 for the three-dimensional flow (E.C.Maskell, 1963). This leads to the final blockage correction formula.

$$C_{Dc} = \frac{C_D}{1 + \epsilon C_D \frac{S}{C}}$$

20

3 Computational Setup

In this chapter, I will cover computational setup such as a CFD program Openfoam, experimental and computational setup, about the new wind tunnel at Universitetet i Stavanger (UiS). This dissertation aims to obtain the first setup of the wind tunnel. By comparing experimental data with the data from CFD, it can give a guideline for further research with the wind tunnel.

3.1 Open-foam

There are many different tools to run CFD, such as Ansys Fluent. However, open-foam is the leading free, open-source software to run CFD.
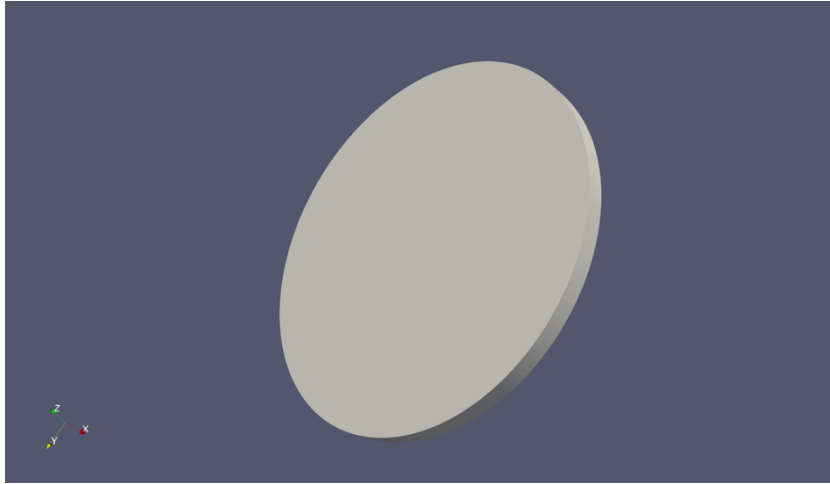
3.1.1   Model

By using Autodesk Inventor, the test section is designed for CFD simulation. Cross section size is 450mm x 450 mm.
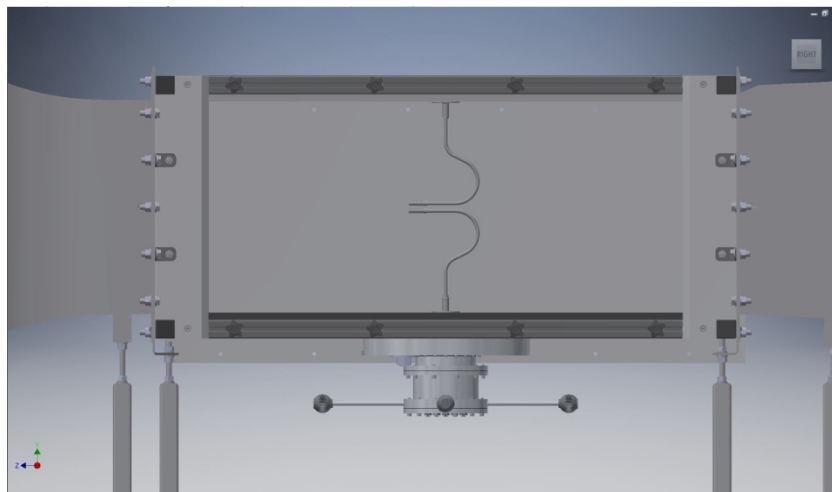
Figure 4. Designed test section

A thin disc is determined as a model to check an object's fluid movement and properties. The diameter of the disk is 100mm.

Figure 5. Disc model

Figure 6 is a designed support model to support an object to stand in the middle of the wind tunnel.

Figure 6. Support for an object

This dissertation also includes the diffuser 1 section to analyze fluid behavior after the test section. Therefore, instead of setting blockMesh as 1250x450x450, 1875x450x450 with 100mm diameter disk has been determined as CFD simulation test region as shown in Figure 7.
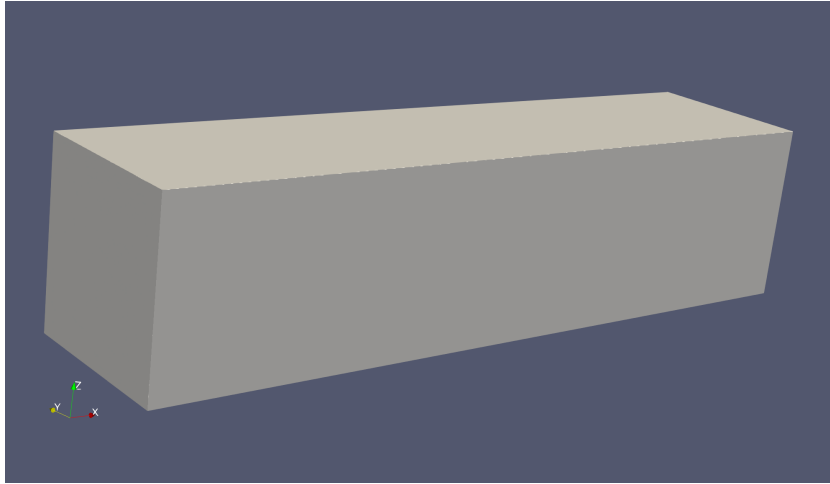
Figure 7. Test region

3.2 Mesh

3.2.1   Boundary layer analysis mesh

blockMesh generates computational multi-block mesh. It is imperative to generate a fine mesh. If not, iteration will not be converged or occur errors. Since the test region is rectangular, which is an elementary geometry, blockMesh is a proper mesh generation utility. Compared to the central part of the test region, parts close to the wall need more detailed mesh. The viscous region is close to the wall, with many changes. For this model, changing values of simple grading have been applied. Default simple-grading is (1 1 1) and (1 8 1), and (1 0.125 1) is applied. This function makes the mesh to be finer, close to the wall section. A cell stick to the wall is eight times thinner than a cell located in the center of the test region. By changing these values, it can have more data close to the wall, which we are interested in. The cross-section is divided into five parts to get finer mesh and more detailed data close to the wall.
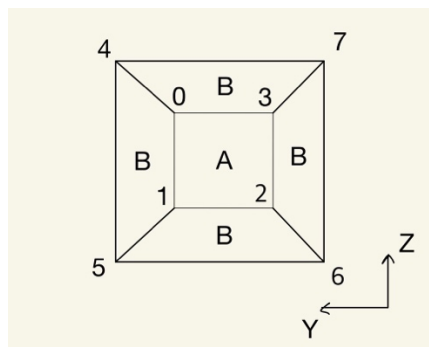

**Figure 8. A simple picture of vertices**

Figure 8 shows a coordinate system for the model. Each vertex is assigned a number. All the numbers were defined through blockMeshDict. In the case of the middle square section, A, it is not a section that

is as important as wall sections. So, it has eight cells each on the edge. Section B must have a finer grid and more grids because it has more detailed data on the wall for boundary layer analysis. Therefore, it has 18 cells along the direction from the square section to the perimeter. After all, these set up for the cross-section mesh, it is able to get mesh picture like Figure 9. In the case of the long side of the pipe, it has been defined $Domain\ lenghth, 1.875m/(\frac{width\ of\ middle\ square\ section, 0.15m}{number\ of\ cells\ in\ the\ square\ section})$. Therefore, 100 cells along the x-axis are assigned. Figure 10 shows the result of meshing along the x-axis. All of the Mesh information is written in the appendix.
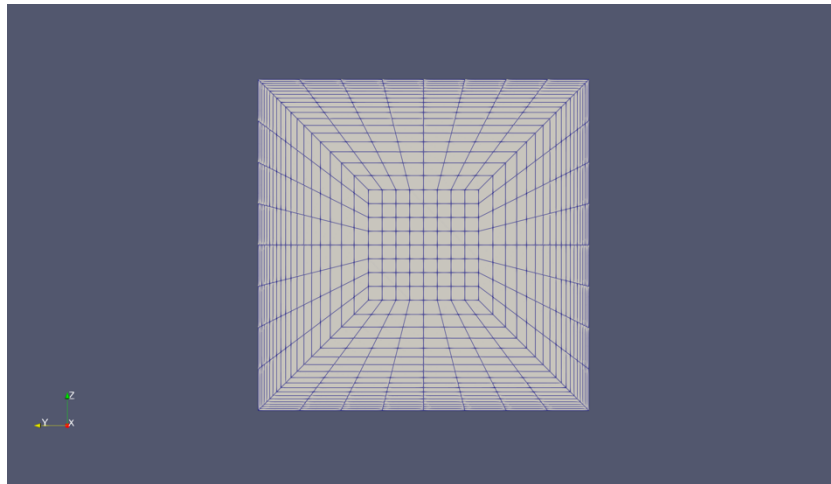
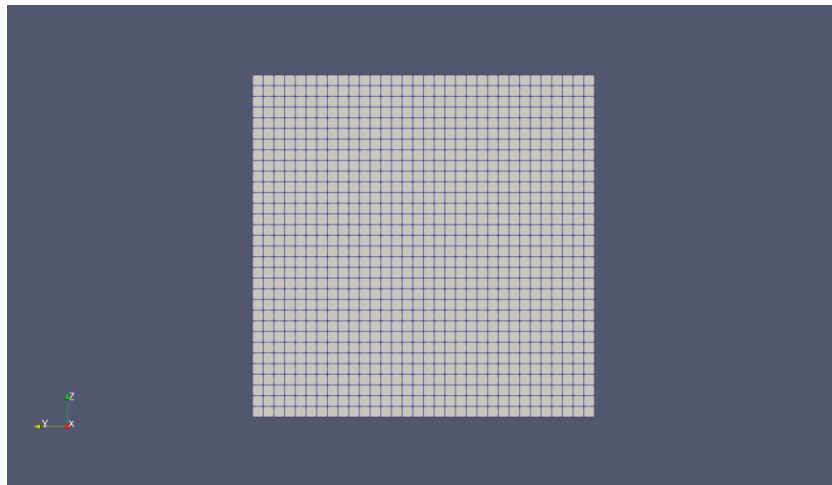**Figure 9. Cross section mesh**
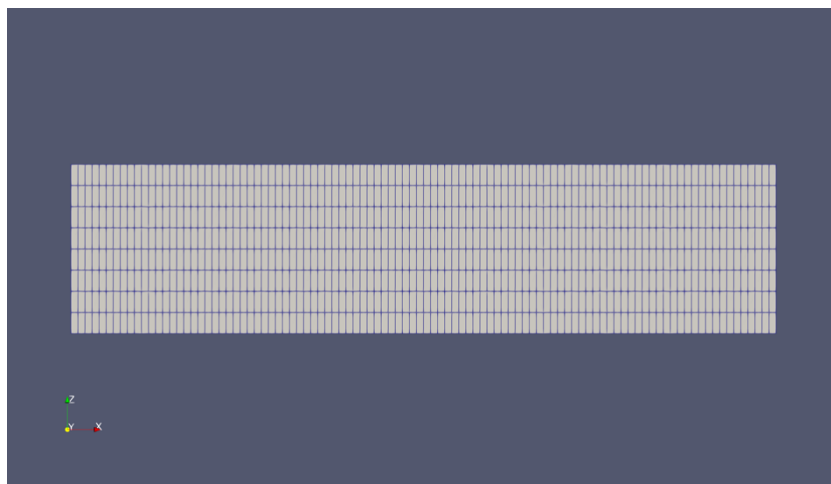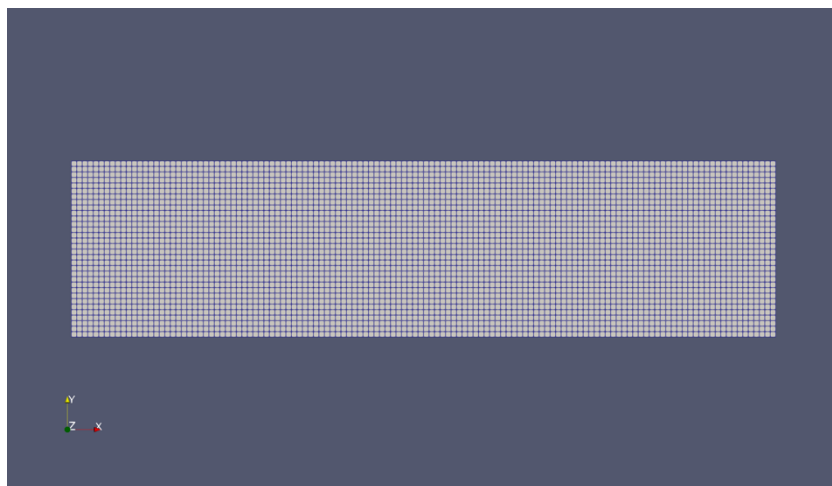

Figure 10. Wall mesh

3.2.2   Grid optimization, wall interference, and supports interference analysis mesh

With finer mesh, as shown in Figure 9, many errors occurred when a disk model and supports were added for snappyHexMesh. If it is too fine, it is able to lose some parts of the mesh close to the wall.

For this reason, a finer mesh is changed to a coarse mesh for this section. Instead of grade scaling, 32 cells to each edge were applied. The edge along the x-axis contains 128 cells.

Figure 11. Cross section mesh

Figure 12. Wall mesh

In this case, finer mesh close to the wall is less important than boundary layer analysis. This is because the disk locates in the middle of the wind tunnel, and only the disk part will be analyzed to obtain the drag coefficient instead of the area close to the wall.

4   Results & Discussion

In this chapter, a thin disk is used as an object to analyze flow movement and force against the model inside the wind tunnel. By changing the mesh size and the ratio between the object and the wind tunnel. To obtain the best result for the wind tunnel unaffected by the wall blockage effect and lack of data. Having fine mesh is important because it is not easy to expect and observe flow tendency close to the object and the wall. After finding the optimized grid size and wind tunnel–object area ratio, supports are added to check the influence of the supports on the disk. Drag difference is observed in two different cases: with supports and without supports.

4.1 Boundary layer analysis u^+ vs y^+

In this chapter, by comparing simulated boundary layer data with theories, validation of the setup will be checked. Flow data inside a pipeline can be obtained using OpenFOAM without any object. This data will be plotted with three equations which were explained in Boundary layer equations. 1/7th Law, log law, and Spalding's Law. To compare these data, changing all data to dimensionalized data u^+ and y^+ has to be done. A program called Paraview is used to show simulated data by OpenFOAM. It is simulated by running code "blockMesh" and "simpleFoam." 296 iterations were executed. To calculate u^+, u* has to be calculated, and it requires a Reynolds number. Universal velocity U is defined as 40m/s, kinematic viscosity ν is defined as $1.516 \times 10^{-5}\ m^2/s$, and domain length x is 1.875m. From these values, $Re_x = 4947230$. Since $Re_x > 3 \times 10^6$, it can be defined as turbulent flow. For turbulent flow, all of the equations that are supposed to compare are able to be applied to be compared with simulated data. According to Boundary thickness, $C_{f,x} = 2.986 \times 10^{-3}$ and u* = 1.5455. u^+ and y^+ are defined in u^+ vs y^+. When the iteration number is 1093, it shows convergence. With this data, chart with u^+ vs y^+ will be conducted.
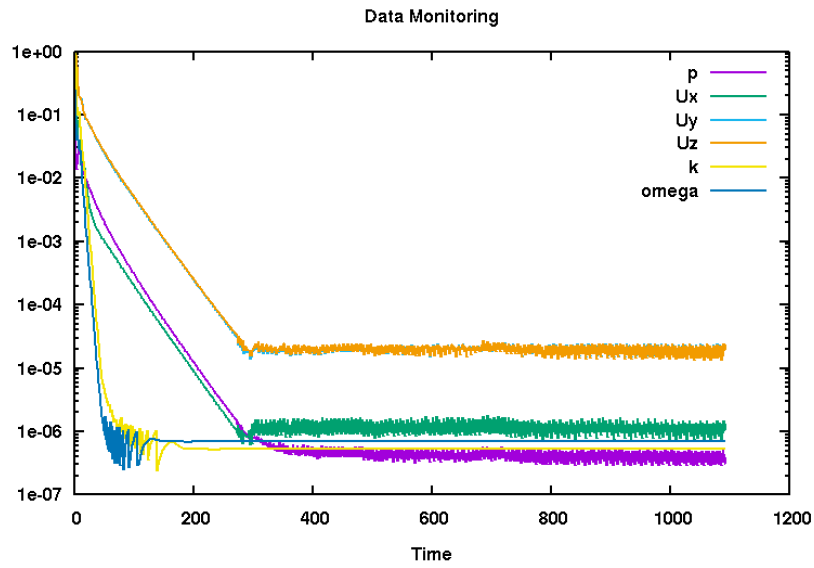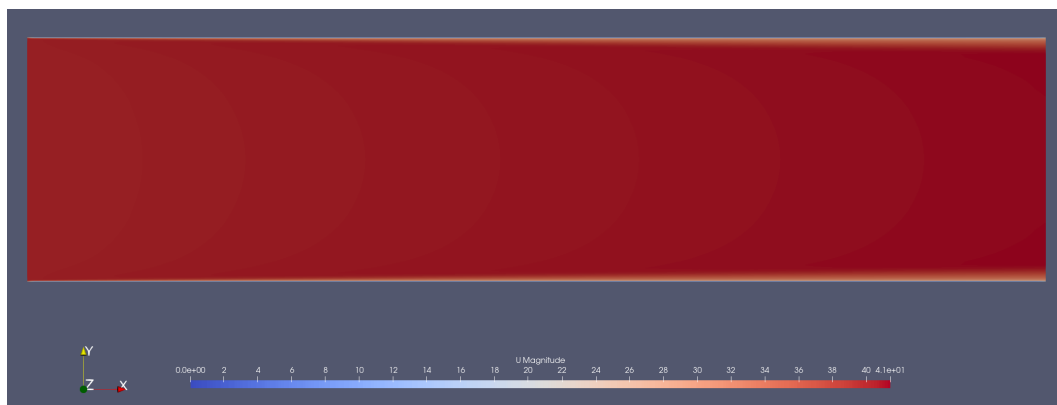
Figure 13. Residual charts

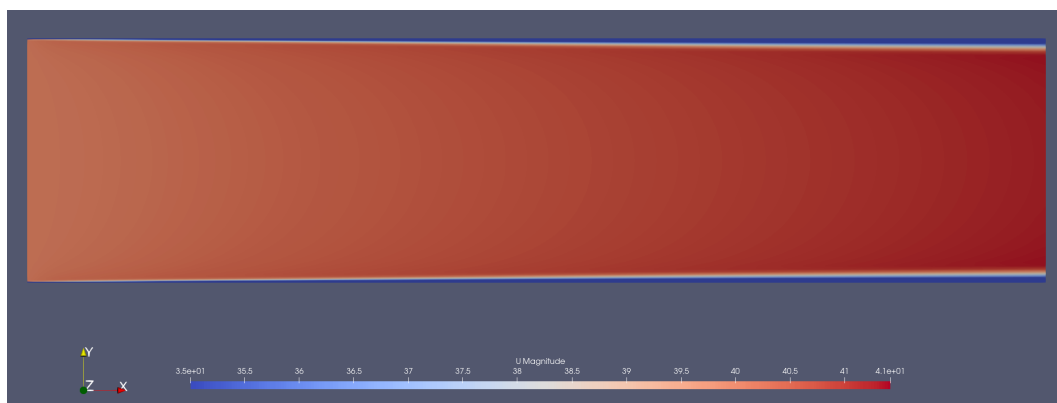**Figure 14. Boundary layer velocity distribution, velocity range 0 - 41m/s**

Figure 15. Boundary layer velocity distribution, velocity range 35 - 41m/s

Figure 14 shows a velocity profile in the test region, and Figure 15 shows how the boundary layer developed along the wall. This shows that the velocity extremely close to the wall is very close to 0.

27

And because of the boundary layer, the area that the universal velocity flow goes through decreases. This occurred gradual velocity increase. Inlet velocity is 40m/s, and outlet velocity is 41.4174m/s. In this chapter, u^+ and y^+ plot will be made at x=0.6 and x=1.8. The reason for choosing x = 0.6 is that objects will locate at x =0.6. For log law, $\kappa = 0.4\ and\ B = 5.0$ are applied.

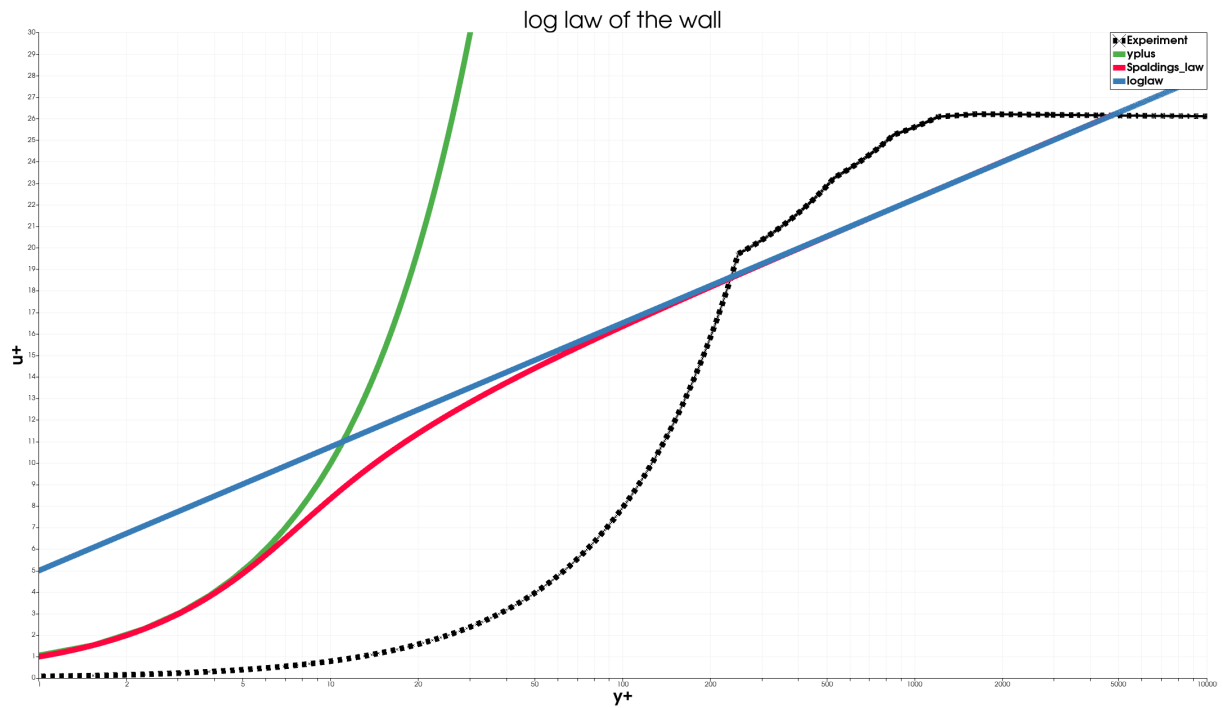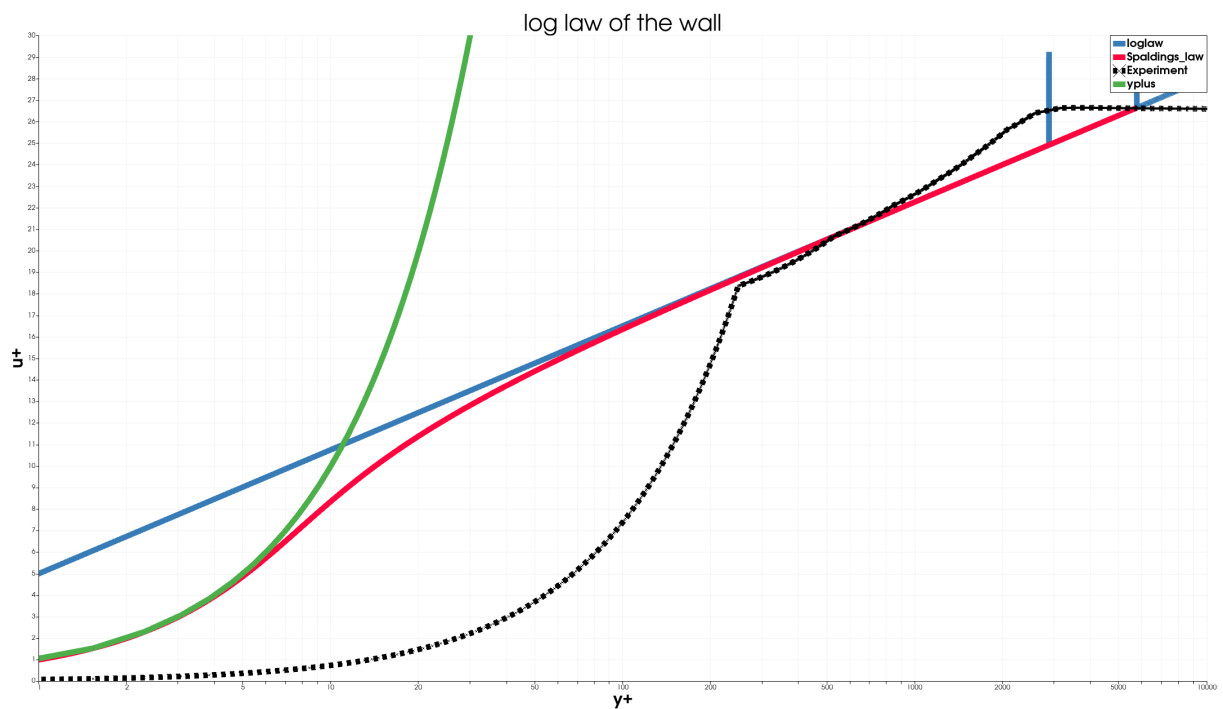**Figure 16. Law of the wall u+ vs y+ at x=0.6**

**Figure 17. Law of the wall u+ vs y+ at x=1.8**

Figure 16 and Figure 17 show the Law of the wall graphs at different locations. Both figures show similar results to Figure 3 when it is not close to the wall. Where y^+ is low, which means it is close to the wall. Simulated data shows the tendency not to follow other laws. Reynold's number in this situation is 4.95×10^7. For Figure 3, it was simulated at $Re_x = 1.0 \times 10^7$. However, when y+ = 220, it started to follow Spalding's law and log law. When y+ = 220, y = 0.00216m. When x =1.8, it shows a more reasonable graph than Figure 16. This is because it is a more developed flow. In Figure 16, simulated data followed Spalding's Law, as same as in Figure 17. This result shows that the wind tunnel's mid-section seems reasonable for conducting further research about a wind tunnel.

4.2 Disk Model

A disk model is used as a base model of this dissertation. Four different mesh sizes are used to check the effect of the grid size. Five different wind tunnel sizes are used to check the effect of the area ratio between the wind tunnel and the object.
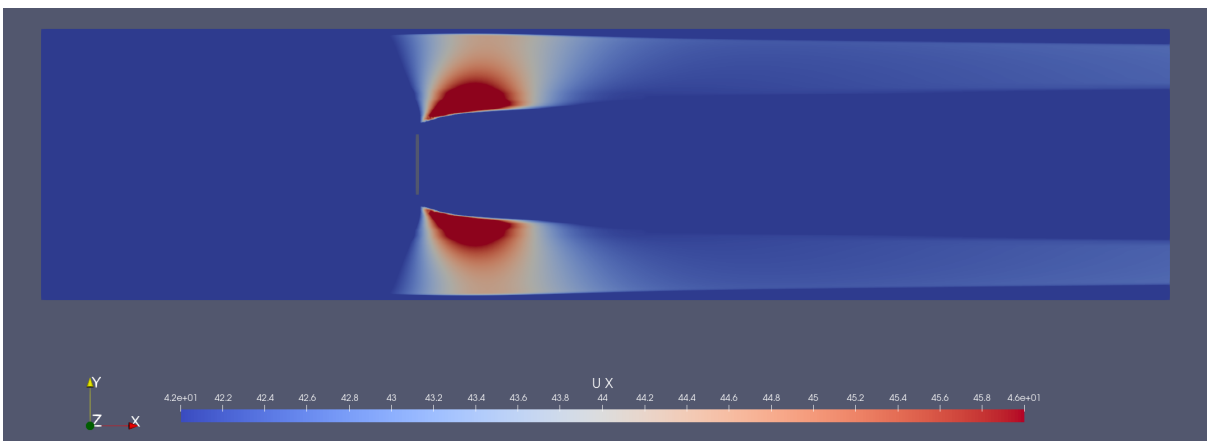
4.2.1 Grid size optimization

The first setup, which was mentioned in [3.2.2], is a base setup for grid size optimization. Each edge parallel to the y-axis and z-axis has eight cells and edges parallel to the x-axis have 100 cells. This is entered in blocks in blockMeshDict. This input was mentioned as (8 8 100), (8 18 100). Moreover, simple base grading is (1 8 1) and (1 0.125 1). To compare different mesh sizes with the same increase ratio, $2^{\frac{1}{3}} \approx 1.26$ is multiplied to blocks and simple grading at every step. The first simulation result was executed with the first set up blocks (8 8 100), (8 18 100) and simpleGrading (1 8 1). The second set up is blocks (10 10 125), (10 23 125), and simpleGrading (1 10 1). The third set up is blocks (13 13 163), (13 29 163) and simpleGrading (1 13 1). The last setup is blocks (16 16 100), (16 36 200), and simpleGrading (1 16 1). The larger the number of blocks and simpleGrading has, the more iteration numbers were needed. The first setup required 296 iterations, the second required 800 iterations, the third required 890 iterations, and the fourth required 1080 iterations to converge.
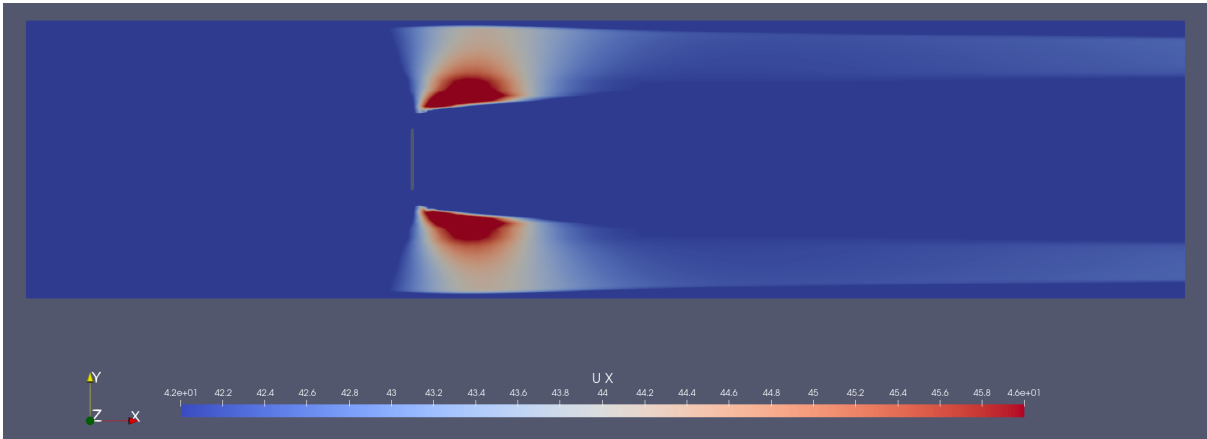
Figure 18. Grid optimization first set up velocity profile (42 ~ 46 m/s)
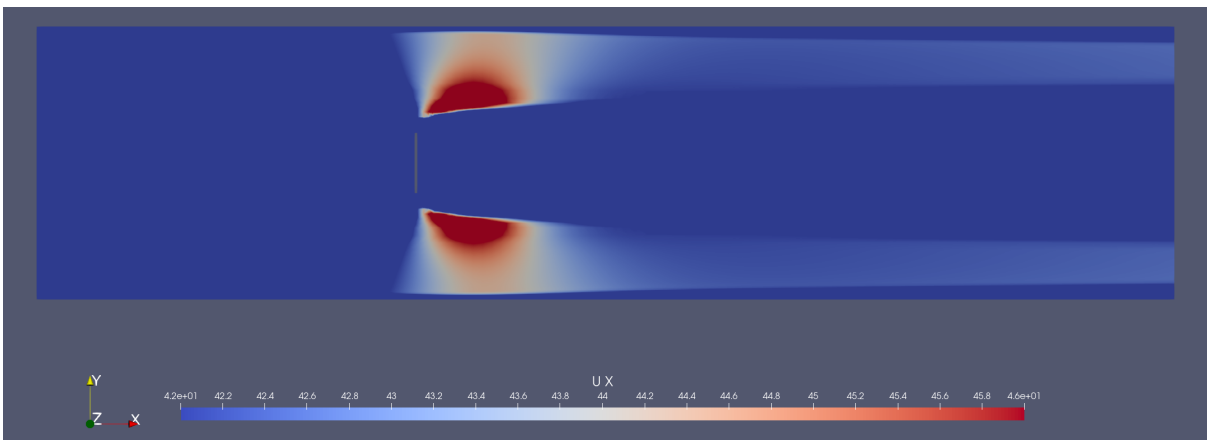
Figure 19. Grid optimization second set up velocity profile (42 ~ 46 m/s)

Figure 20. Grid optimization third set up velocity profile (42 ~ 46 m/s)
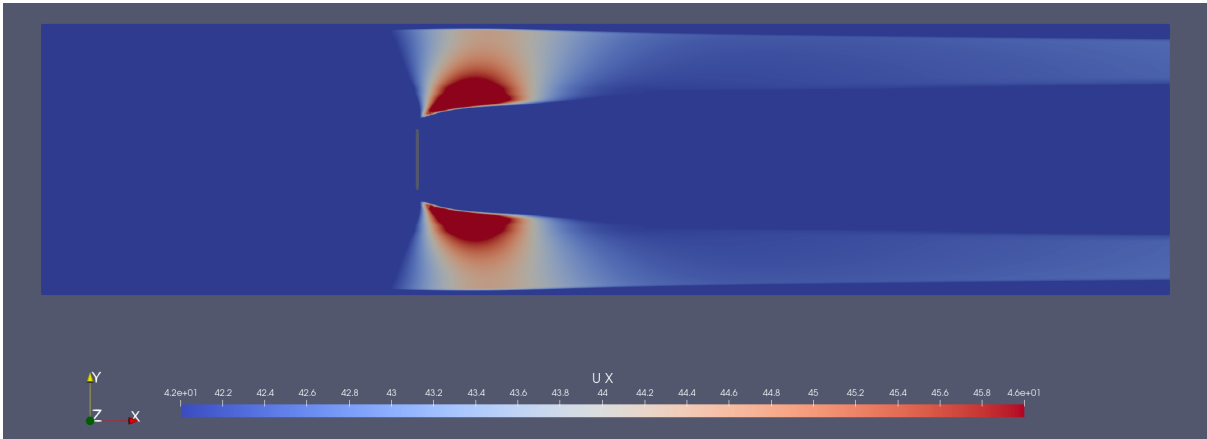
Figure 21. Grid optimization fourth set up velocity profile (42 ~ 46 m/s)

Model	Drag coefficient C_D	Difference	Corrected C_D
First set up	1.365	0%	1.205
Second setup (1.26 times finer)	1.389	1.79%	1.224
Third setup (1.59 times finer)	1.368	0.28%	1.208
Fourth set up (2 times finer)	1.365	0.04%	1.206

**Table 1. Drag coefficient with different gird size**

Figure 18, Figure 19, Figure 20, and Figure 21 show the velocity profiles of different grid sizes set up around the disk model. The legendary range was assigned to 42 ~ 46m/s instead of 0 ~ 46m/s because of the very small difference between the models. The four models do not show any significant difference in velocity and pressure. As the simulated result has a finer grid size, the velocity profile seems to be a softer result. Table 1 shows the apparent results. Grid size did not affect the drag coefficient C_D. Even though the fourth setup has twice the finer grid size, the drag coefficient was changed by only 0.04%. All the differences between the first and the other setup are less than 2%. In the case of the corrected drag coefficient values, it shows the blockage correction method well since it is closer to the theoretical value than the measured drag coefficient values in Table 2. This leads to the result that grid size does not affect the result. As a result, the first setup is suitable for further research.

4.2.2   Different ratios of tunnel size and disk

This chapter searches the optimized ratio of tunnel size and the disk. The biggest issue with using a wind tunnel is that it is not perfect as same as the actual environment. When people do experiments about flow movement with wind tunnels, they consider it will be applied to open space. However, a wind tunnel is a closed space. So, it will be affected by the walls of a wind tunnel. Simulations with five different models were carried out to check the ratio of tunnel size, and the disk does not affect the result and can be assumed as open space. blockMesh size was increased by 0%, 20%, 50%, 100%, and 150% for this simulation. The length of each edge is 450mm, and the diameter of the disk is 100mm.

31

The area ratio of each model is 3.88%, 2.69%, 1.72%, 0.97%, and 0.62%. To see how the wall affects the result, the pressure range is determined to be -200 ~ 200 Pa, and the velocity range is determined to be 36 ~ 49m/s. In order to have a reasonable result with the increasing length of the edge, the number of cells along the edge was also increased with the same ratio. All the models converged when the iteration number was 270 ~ 290.
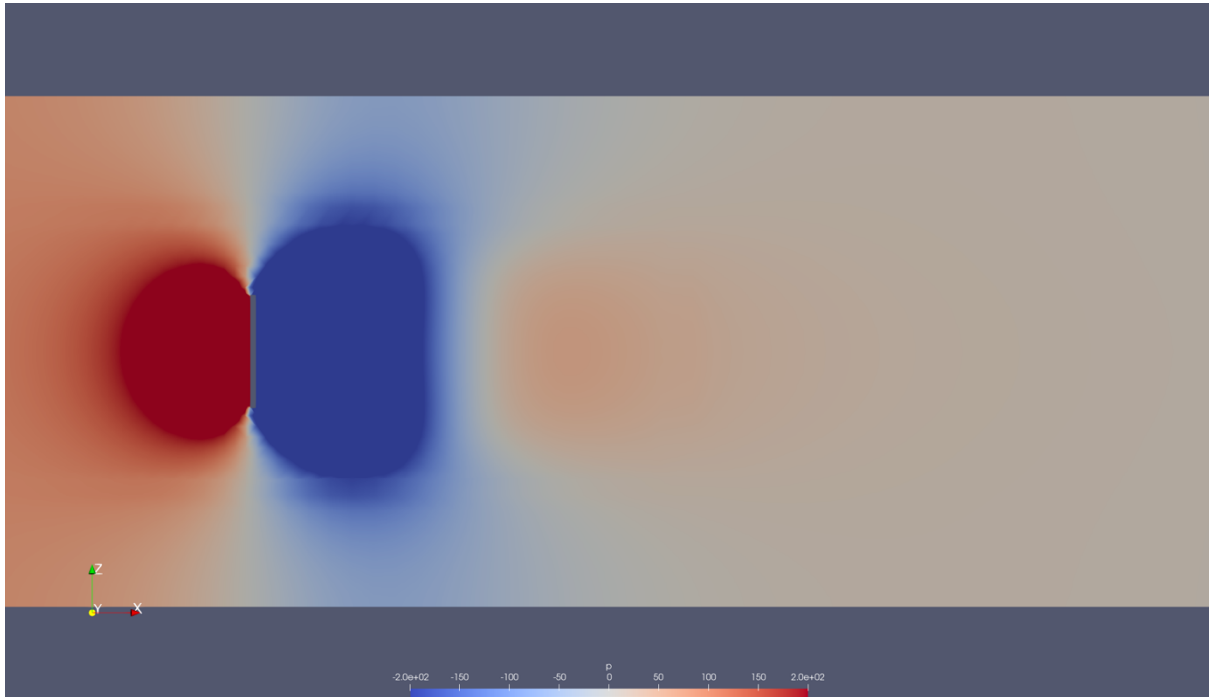
Figure 22. Pressure profile of first set up, 0% increased, (-200 ~ 200 Pa)
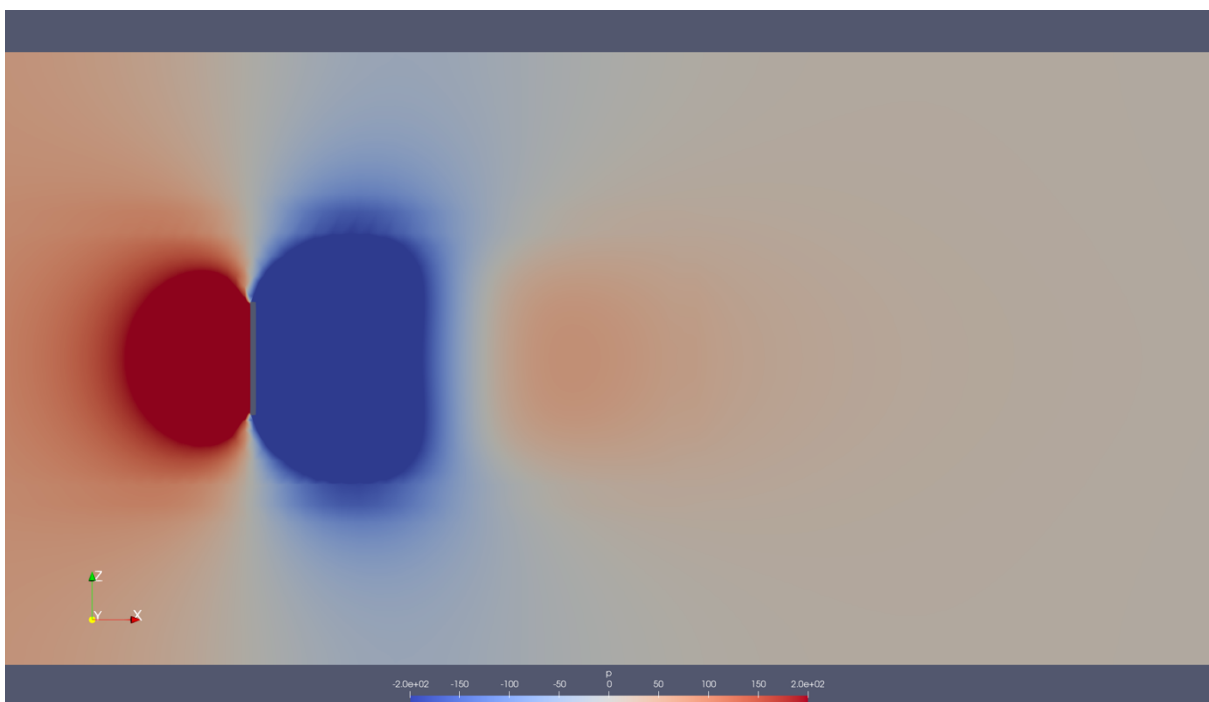
Figure 23. Pressure profile of first set up, 20% increased, (-200 ~ 200 Pa)

32
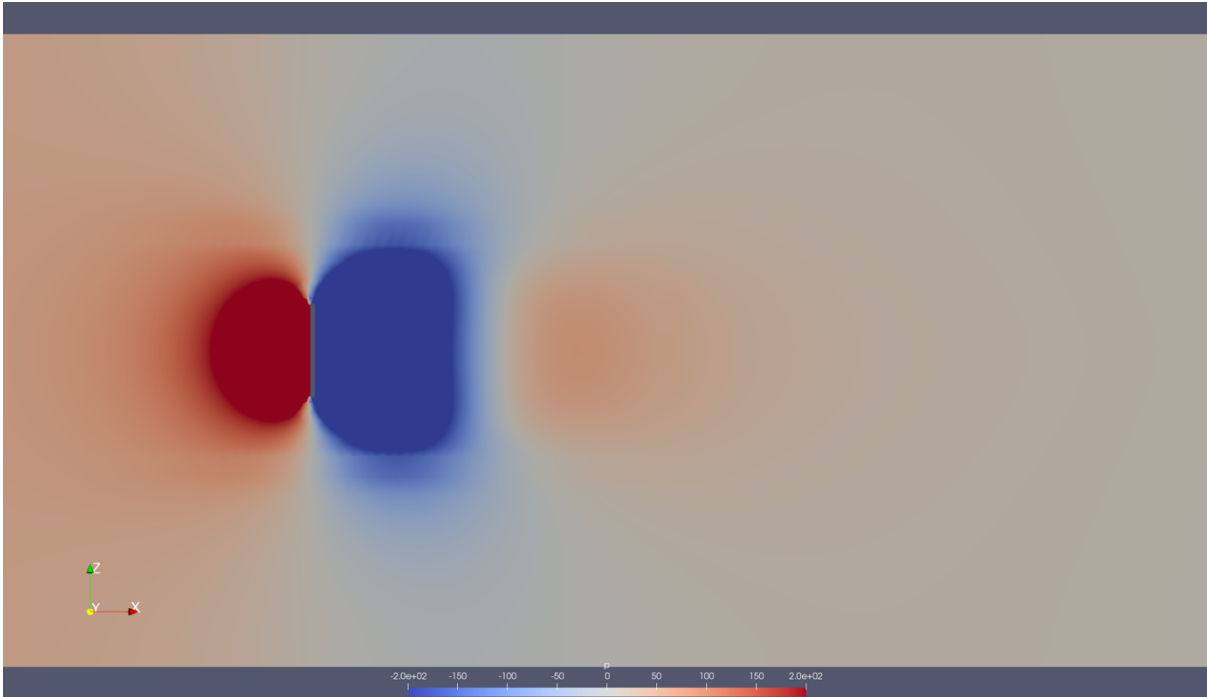
Figure 24. Pressure profile of first set up, 50% increased, (-200 ~ 200 Pa)
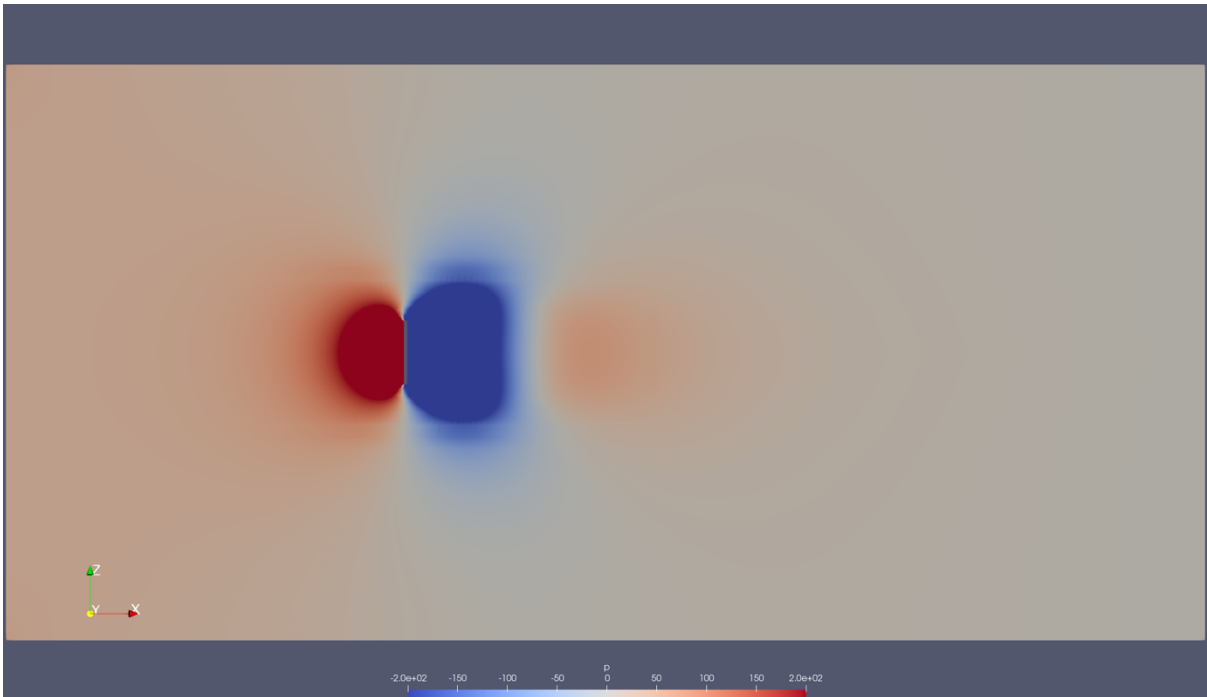
Figure 25. Pressure profile of first set up, 100% increased, (-200 ~ 200 Pa)
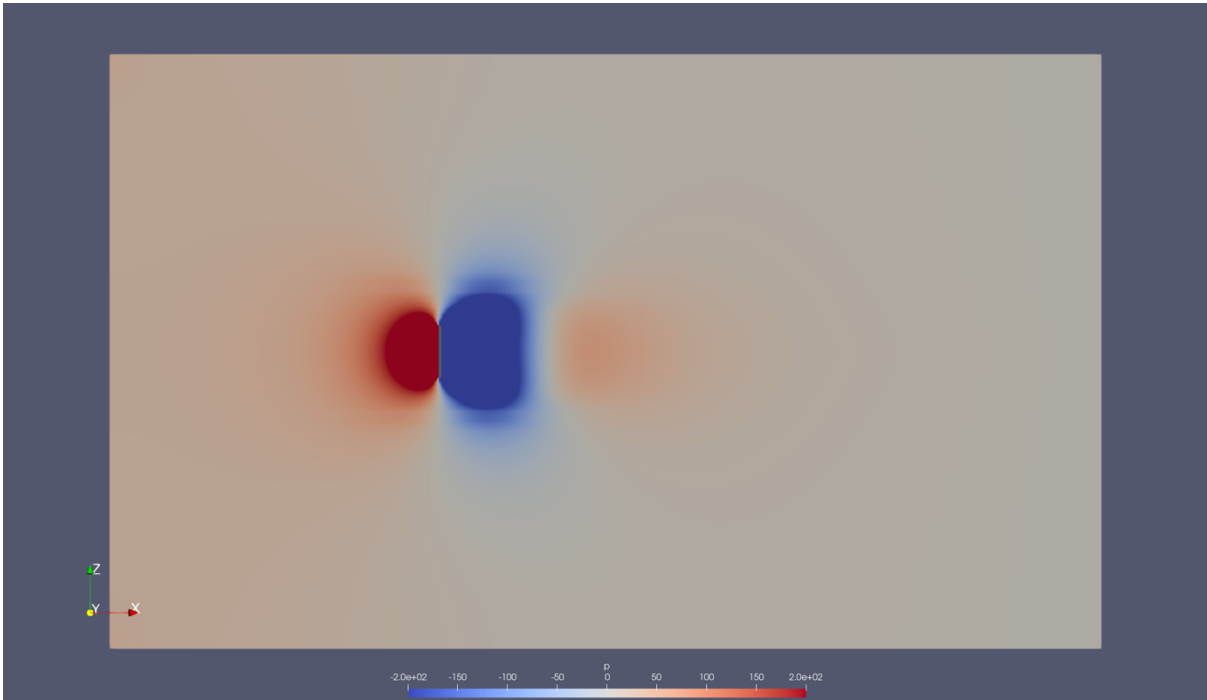
Figure 26. Pressure profile of first set up, 150% increased, (-200 ~ 200 Pa)
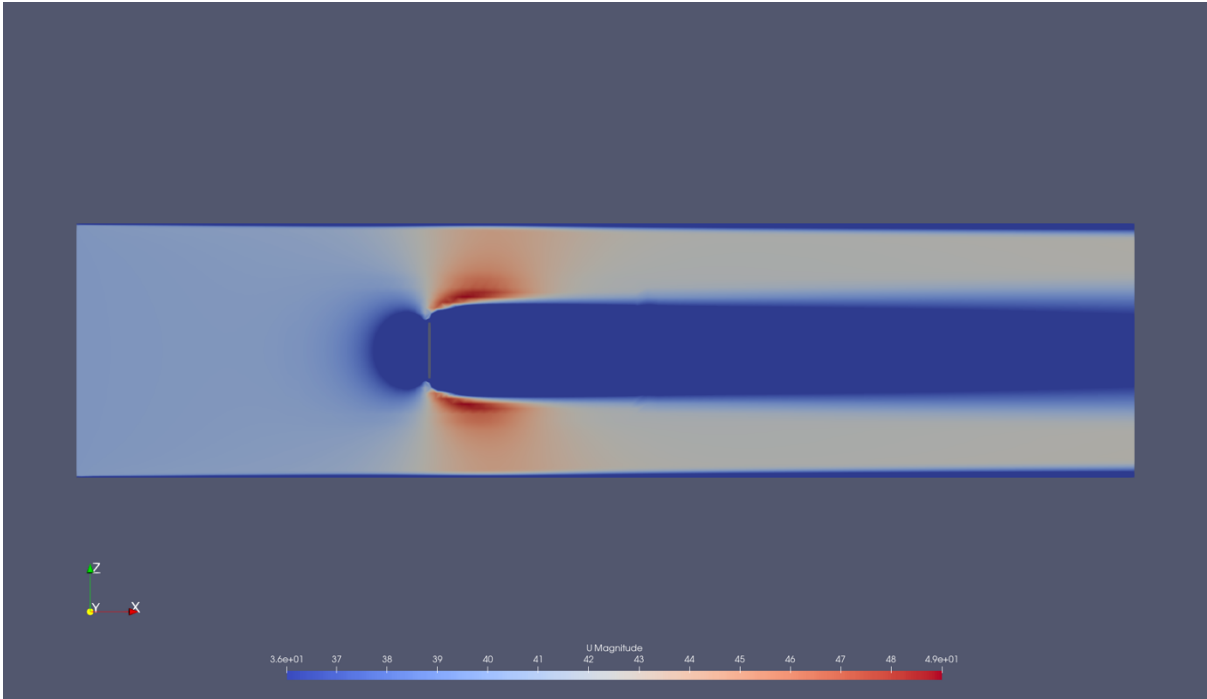
Figure 27. Velocity profile of first set up, 0% increased, (36 ~ 49 m/s)

34
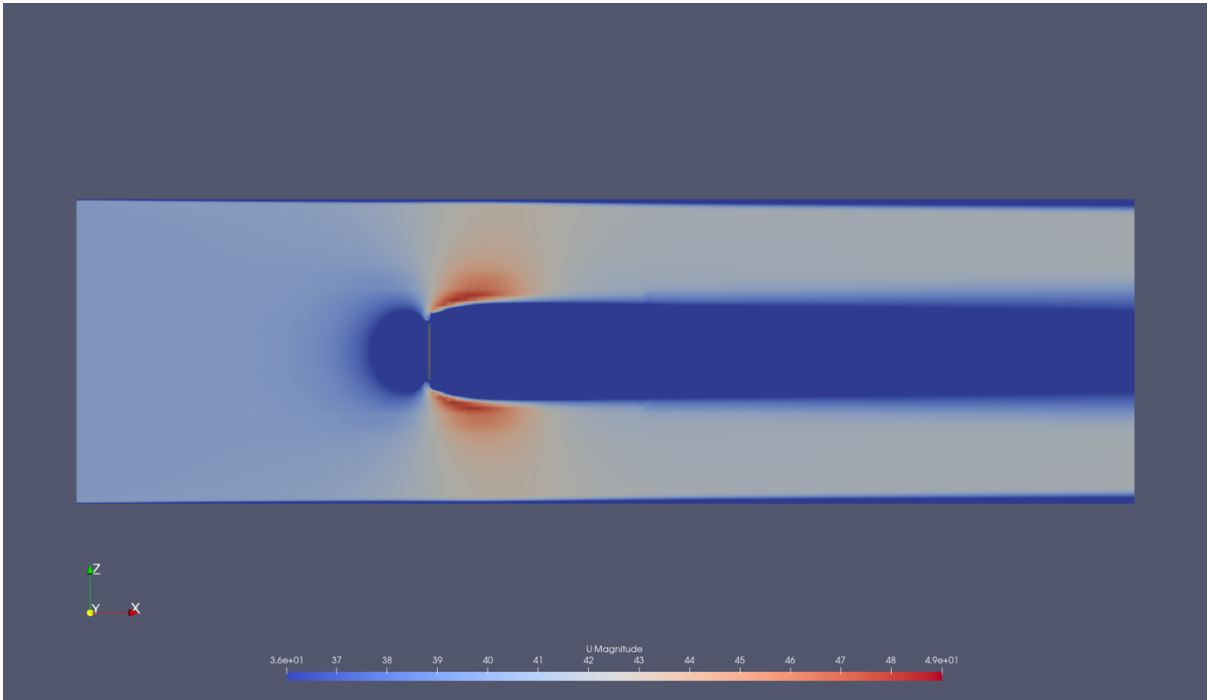
Figure 28. Velocity profile of first set up, 20% increased (36 ~ 49 m/s)

Figure 29. Velocity profile of first set up, 50% increased (36 ~ 49 m/s)

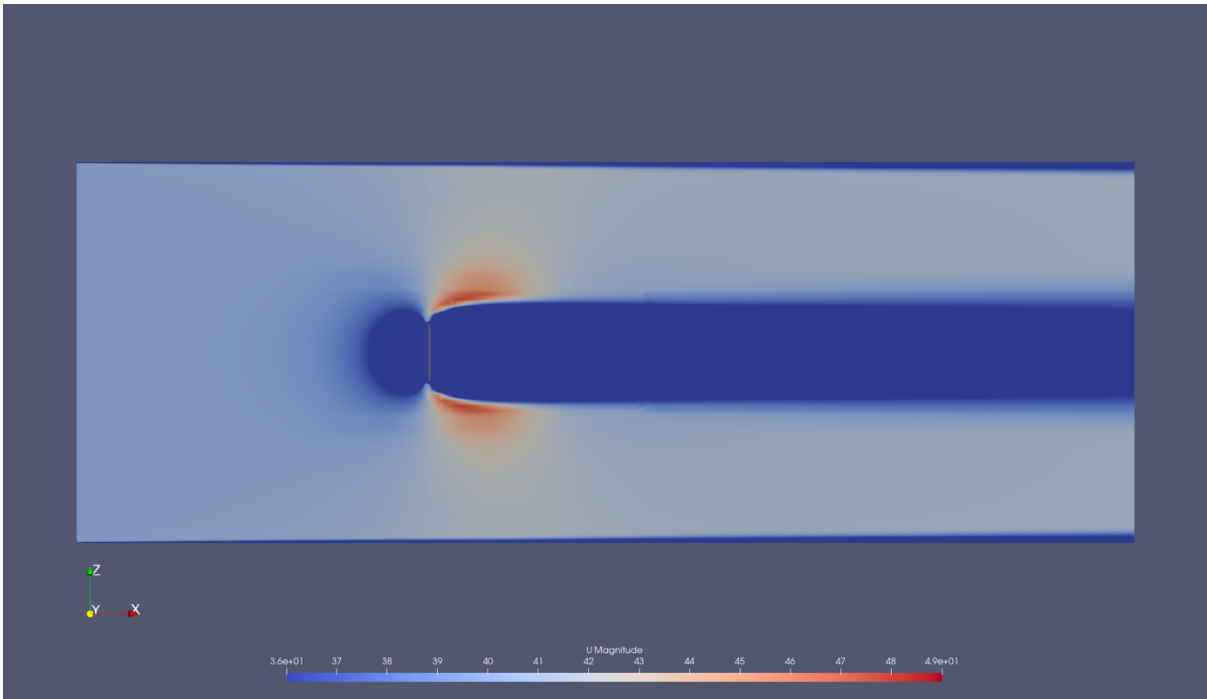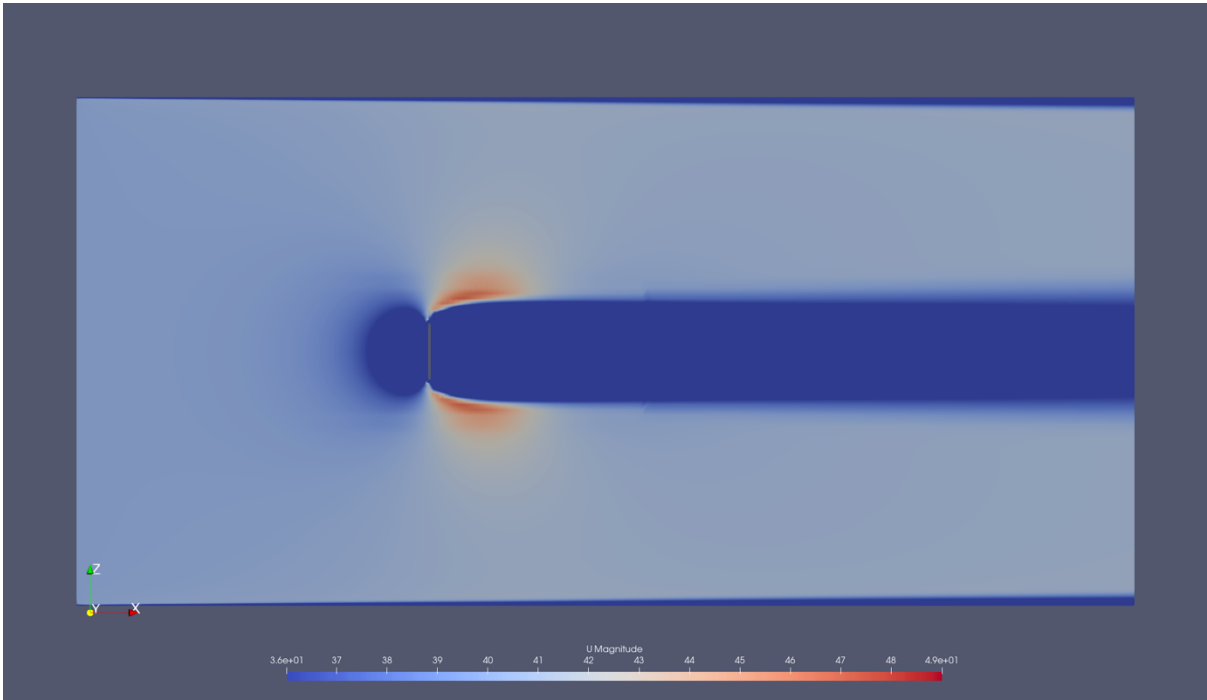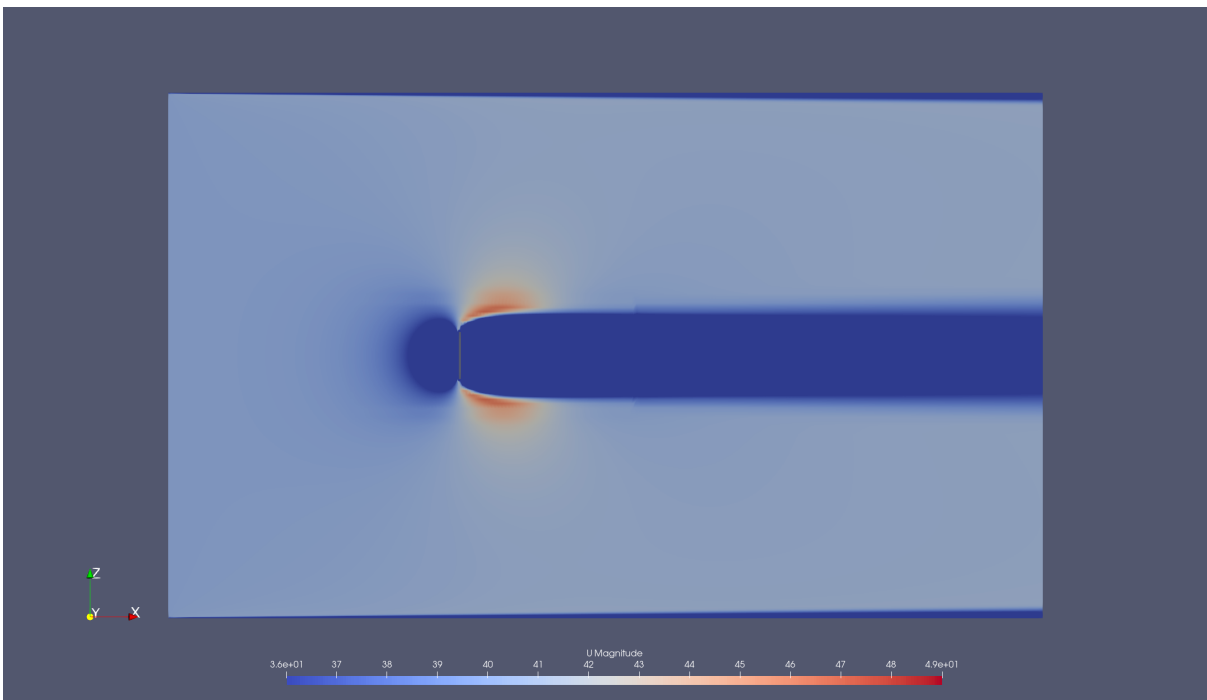**Figure 30. Velocity profile of first set up, 100% increased (36 ~ 49 m/s)**

Figure 31. Velocity profile of first set up, 150% increased (36 ~ 49 m/s)

Model	Drag coefficient C_D	Difference	Corrected C_D
First set up	1.365	0%	1.205
Second set up (20% increased)	1.389	-3.17%	1.270
Third set up (50% increased)	1.274	-6.62%	1.208
Fourth set up (100% increased)	1.247	-8.59%	1.211
Fifth set up (150% increased)	1.229	-9.92%	1.206

Table 2. Drag coefficient with different wall distances

Compared to the grid optimization, changing the cross-sectional area of the wind tunnel showed a significant change as the length of the edge increased. Figure 22, Figure 23, and Figure 24 it was able to detect that the blue area, which has low pressure, is distributed close to the wall and is affected by the wall. However, in Figure 25, and Figure 26, it is not affected by the wall. These two figures show very similar results. Moreover, Figure 27 shows that the high-velocity region right behind the disk model is more significant than other figures. According to Bernoulli's equation and continuity equation, the area of the entrance that the flow goes through affects the velocity if the pressure difference is very small and the height location is the same. Because of the wall blockage effect, the area that the flow goes through becomes narrow, so the velocity becomes higher, and the pressure is comparatively low. Moreover, in the case of Figure 27, Figure 28, and Figure 29, the flow which has passed the disk and locates in between the wall and middle flow shows more yellow color, which means it has higher velocity distribution. This was also affected by the small area of the wind tunnel cross-sectional area. Table 2 shows significant results with numbers. According to the Drag Coefficients of common geometries, the drag coefficient C_D of the disk is 1.1. The default model had a higher drag coefficient because of the wall blockage effect. As significant as the wall distance increased, drag coefficient values decreased and became close to the theoretical value of 1.1.

Moreover, it is able to check that the corrected drag coefficient is very close to the theoretical drag coefficient. Maskell's method applies very well to this simulation. Even though having more space between the wall and the model, it could not reduce as much as the blockage correction did. After blockage correction in all cases, all the values showed similar values. With all these results, I was able to have a conclusion that the area ratio between the wind tunnel and the object affects to the result, and the ratio of less than 1% can be considered as open space.

4.3 Support interference effect

In this chapter, support interference has been observed. Three models were used to be compared. The first model is a disk without any support. The second model is a disk with support. The last model is a disk with two supports. For this section, a different blockMesh was applied because simpleGrading occurred some problems. Since it was too fine, snappyHexMe did not work correctly, and some parts

of the support model close to the could not have proper mesh. It showed as an empty space. For this case, simpleGrading was not applied. Instead of simpleGrading, (8 8 100) and (8 18 100), (128 32 32) was applied. As long as the area close to the wall is not very important in this section, having the same gird size is reasonable.

Pressure distribution, velocity distribution, and drag coefficient were obtained and compared to analyze how the support affects the disk. According to the verification of wind tunnel model support and wall interference assessments in DNW-HST by CFD simulations (Frenk & Hans, n.d.), the strut and supports affected the drag coefficient. The drag coefficient increased even though the difference between the model with and without supports is very small. This is because the support can occur turbulence, and this can affect the airflow around the model. This turbulence and interference with the airflow can lead to obtaining imprecise results. Therefore, it is crucial to consider how to design the support structure so that it does not interfere with the airflow around the test model. If the support is thin enough, it will affect less because it may have a negligible impact on the test model. So, the thickness of support, the roughness of support, and the well-aligned support are important to reduce the impact of the supports on the test model. If it is not installed correctly, turbulence and flow separation may occur, affecting the drag coefficient. Furthermore, it can induce interference effects with the boundary layer on the disk model.

In order to compare the drag coefficient and observe how the supports affect the drag coefficient, all cases were applied with the same conditions. The same blockMesh, snappyHexMesh, and controlDict were applied. All data showed that they converged around iteration number 400. So Convergence iteration number was set up to 2000. The drag coefficient C_D was obtained by using Python.

The diameter of the disk is 0.1m. Therefore, The area of disk A is $A = \frac{1}{4} \times 0.1 \times 0.1 \times \pi = 0,00785398 \ m^2$. Drag coefficient C_D is obtained by dividing $C_D A$ by the area of disk A.

Model	$C_D A \ [m^2]$	Drag coefficient C_D	Difference
Disk	0.0108	1.369	0%
Disk with a one support	0.0105	1.334	-2.59%
Disk with two supports	0.0104	1.322	-3.48%
Supports	0.00234	-	-

Table 3. Drag coefficient comparison
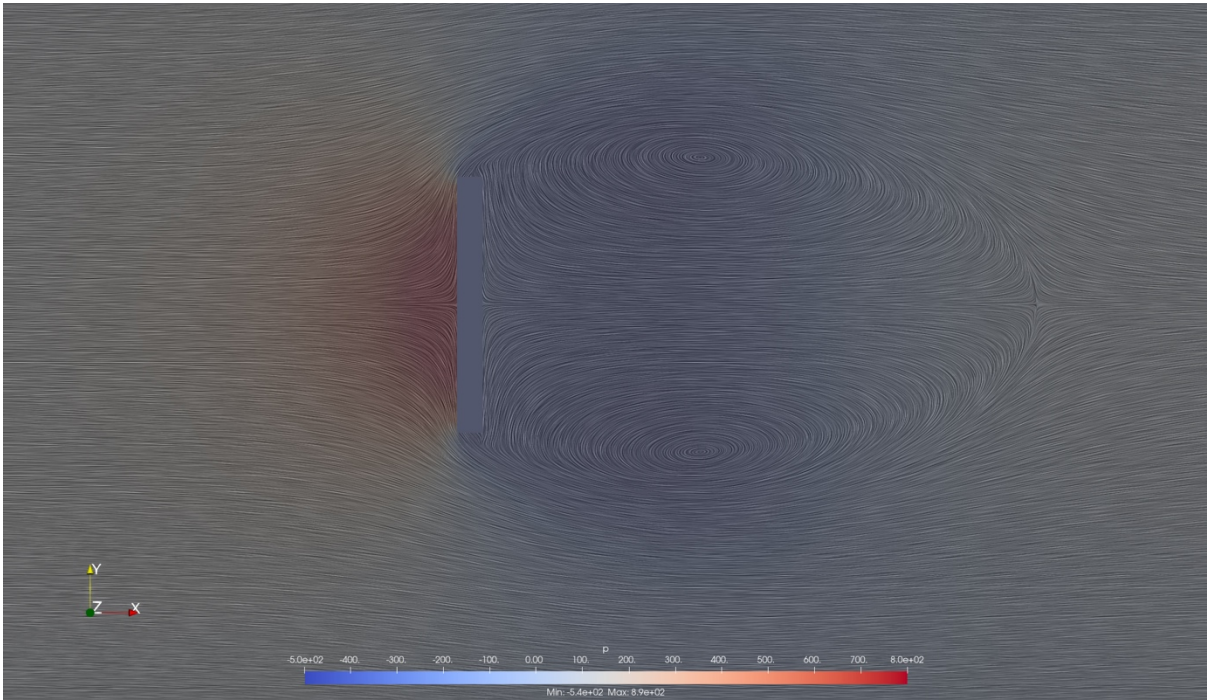
Figure 32. The pressure vector field of a disk without support
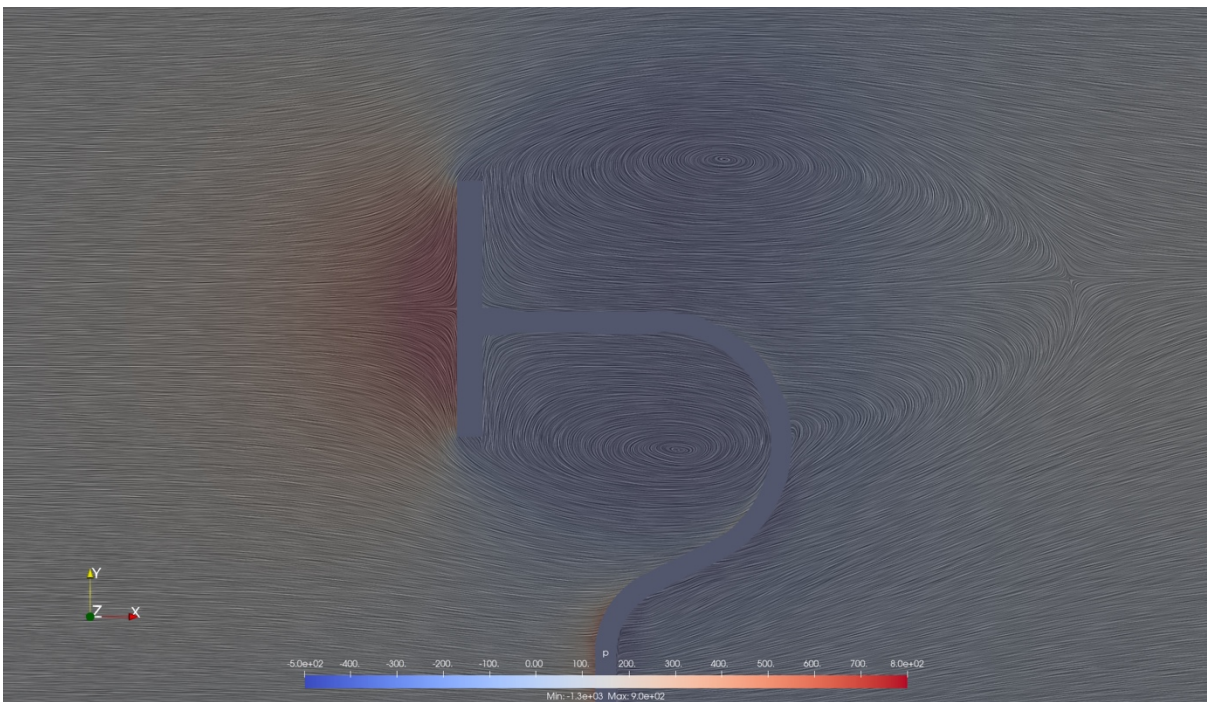
Figure 33. The pressure vector field of a disk with one support
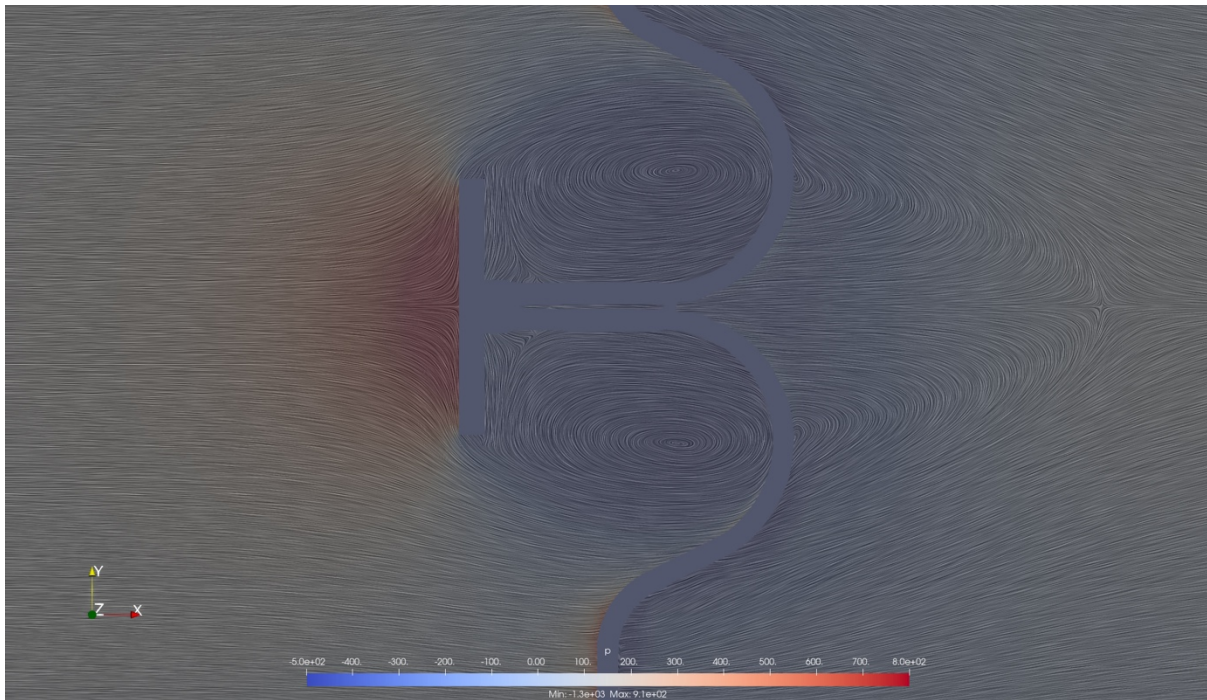
Figure 34. The pressure vector field of a disk with two supports

According to Table 3, the drag coefficient decreased as many supports were added. According to (Sims-Williams, 2004) drag coefficient tend to increase by at least 1% because of the support interference. However, it also mentioned that this change depends on which type of support was used. The location of the supports makes a big difference as well. Frenk and Edgard mentioned that because of the possible data uncertainty, it is very important to apply error correction to obtain precise absolute drag values from wind tunnels (Frenk & Hans, n.d.). Moreover, they mentioned that the level of support interference corrections depends on the test setup, which can affect the order of $10 \sim 20\%$ of the minimum drag value. The increment of the Drag coefficient in these references was concluded because of undesired flow distortion developed at the end of the edge. This flow distortion is generated by the formation of horseshoe vortex structure (Corte, et al., 2019).

However, Table 3 and Figure 32, Figure 33, and Figure 34 show the opposite result. Many factors reduce the drag coefficient of the model. They are the model's geometry, the air's motion, and the air's properties (NASA, n.d.). In this case, the motion of the air affected the decrement of the drag coefficient. Figure 33 shows a different flow pattern. The support is stuck to the downside, with no upside-down support. By checking streamlines that describe how the airflow passes through the wind tunnel, it was able to check the wake location and its scale. The wake scale can affect the model's drag coefficient inside the wind tunnel. Figure 33 shows the difference in the wake scale between those without and with support. The scale of the wake when there is no support is larger and thicker than the scale of the wake when there is support. According to (Caltech, n.d.), the connection between drag and the wake can be explained by using the momentum equation. This showed that the larger wake could generate a larger drag. A thinner wake reduces the applied drag force against the model. In this case, the best example is

40

a golf ball with many dimples (Peter E. Jenkins, 2018). The reason for the size change of the wake behind the disk is that the support interrupts the development of the vortex. When there are no supports, the wake is generated without any interruptions. However, the supports are located in the middle of the wake. These supports divided and interrupted the development of the wake.

Furthermore, the location of isolated stagnation points, which locates behind the disk and the end of the wake flow, has been changed. As the wake size becomes smaller with supports, the stagnation points are slightly moved away to the right from the disk and the supports when there is only one support. As in Figure 33, a stagnation point moves slightly up to the space where the support does not exist. As well as the change in the location of isolated stagnation points, each case's minimum and maximum pressure were changed. The minimum pressure of each case is -544 Pa, -129,8 Pa, and -1321 Pa. Maximum pressure of each case is 893 Pa, 900 Pa, and 908 Pa. As much support the model has, the maximum pressure increased, and the minimum pressure decreased. In the case of (Aurélia Cartieri, 2012), (Frenk & Hans, n.d.), models are attached to the extended support, perpendicular to the model and horizontal to the wind tunnels. So the supports do not affect the wake formation. If the part of the supports connected to the model perpendicularly becomes longer so that it does not affect the wake formation, it would give more reasonable results with fewer errors.

Because of the support interference developed by wake development interruption, pressure changes, and location change of the isolated stagnation point, the result obtained from this simulation is that the drag coefficient of the disk model decreased. When an object moves, the object experiences a pressure difference between the front and behind parts because of the creation of a disturbance in the flow. This occurs through drag force on the object. Moreover, the strut or strings that hold the object alter the pressure difference around the object. Moreover, the boundary layer is developed along the supports. This increased the pressure on the back of the disk. This pressure difference change reduced the effectiveness of the backward-facing step, which created a large separation bubble and increased drag on the back of the disk. A larger wake means there is more resistance to the object's movement through the fluid. This led to the overall drag reduction.

With all these results, installing supports will decrease the model's drag coefficient. However, it depends on the location of the supports, the geometry of the support, and the surface property of the supports. Many factors can affect the support interference impact against the disk model.

5 Conclusion

Wind tunnel testing is a machine to expect how fluid flows will flow over and along the object. Since it is impossible to obtain perfect theoretical results from the Navier-Stokes equation, accurate results are obtained by many iterations and simulations. This is how computational fluid dynamics is used to expect many aerodynamic occurrences, such as anticipating weather and improving airplane efficiency. To have the first setup of a new wind tunnel at Universitetet i Stavanger, comparing empirical data and simulated data was needed. To obtain a reasonable setup, verifying the law of the wall was conducted first. Simulated data followed Spalding's law when analyzed close to the wall. At a certain point where it is enough away from the wall, it followed log law and $1/7^{th}$ law. This result showed agreement with the theory.

After the boundary layer verification, grid optimization and wall distance effect were checked. For the grid optimization, the grid size was 1.26 times finer every time. It was conducted until the grid size became half from the first setup. And there was no significant change. Pressure, velocity, and drag data did not change a lot. The drag coefficient difference range was less than 2%. In the case of the wall distance effect, it showed a noticeable result. Wall distance has been increased to 120%, 150%, 200%, and 250%. Every time the wall distance increased, the wall blockage effect on the object reduced. In the case of 200% increased case and 250% increased case, pressure and velocity distribution close to the disk model were very similar to each other cases. The larger the wall distance increases, the drag coefficient becomes closer to the theoretical value. From this, it was able to check that grid size does not affect the results, and the wall distance affects the results largely because of wall interference with the disk model. Lastly, support interference was checked. This was conducted with four cases: only disk, disk with one support, disk with two supports, and supports without the disk. Pressure distribution, vector field, and drag coefficient difference were analyzed for the support interference check. This is because the drag coefficient is affected by pressure difference. The change in the scale of the wake happened because of the support. Supports disturbed the development of the vortex behind the disk. This affected the pressure difference between the front part of the disk and the behind part of the disk. Because of this support interference, the drag coefficient decreased when the supports were installed. However, some references mentioned that the drag coefficient increases. These references are used to support which is connected to the wall, and the connected part was located far away from the test object. Therefore, it did not affect the wake formation behind the back space of the disk.

This leads to the conclusion that the wall interference and the support interference affect the drag value of the test object. So interference correction is needed to get more accurate and reasonable results to compare with the empirical data.

References

[1] Yunus A.Çengel, J. M., 2010. *Fluid Mechanics Fundamentals and Applications.* 2 ed. s.l.:McGraw-Hill.

[2] Centrum Techniki Okrętowej S.A., 2023. *User manual,* Gdansk: Centrum Techniki Okrętowej S.A..

[3] Liu, F., 2017. *A Thorough Description Of How Wall Functions Are Implemented In OpenFOAM.* s.l., Chalmers university of techology.

[4] Ernad, B., Samir, L. & Fuad, H., 2020. *Procedure for Determining the Wind Tunnel Blockage Correction Factor.* s.l., University of Zenica.

[5] Atsushi, . H. & Masataka, . K., 2012. *Wall Interference Analysis by Whole Wind Tunnel CFD Atsushi Hashimoto.* Tokyo, Japan Aerospace Exploration Agency.

[6] Jewel, B. B., William, R. H. & Alan, P., 1997. *Low-speed wind tunnel testing.* 3 ed. s.l.:JOHN WILEY & SONS, INC.

[7] Frenk, W. & Hans, M., n.d. *Verification of wind tunnel model support and wall interference assessments in DNW-HST by CFD simulations,* s.l.: NATO.

[8] Sims-Williams, B. H. a. D. B., 2004. *Wind Tunnel Model Support Strut Interference,* s.l.: SAE International.

[9] Corte, B. D., André, A., Martijn, . v. S. & Arvind, . G. R., 2019. *Experimental and Computational Analysis of Model–Support Interference in Low-Speed Wind-Tunnel Testing of Fuselage-Boundary-Layer Ingestion,* Delft: Delft University of Technology, Faculty of Aerospace Engineering.

[10] S Russo, J. M. J. A. N. P. S. A. L. P. R.-C., 2020. *A CFD study on the strut interference on a regional aircraft wind-tunnel model ,* s.l.: IOP.

[11] NASA, n.d. *Glen Research Center.* [Online]
Available at: https://www.grc.nasa.gov/www/k-12/VirtualAero/BottleRocket/airplane/factord.html

[12] Caltech, n.d. *The Connection between Drag and the Wake.* [Online]
Available at: http://brennen.caltech.edu/fluidbook/externalflows/drag/dragNwake.pdf

[13] Peter E. Jenkins, J. A. M. R. M. S., 2018. Drag Coefficients of Golf Balls. *World Journal of Mechanics,* 6(8).

[14] Aurélia Cartieri, P. V. S. M., 2012. *Using CFD to calculate support interference effect in wind tunnel tests.,* Paris: HAL open science.

[15] CFD online, 2011. *SST k-omega model.* [Online]
Available at: https://www.cfd-online.com/Wiki/SST_k-omega_model
[Accessed 28 2 2011].

[16] AUTODESK, n.d. *SST K-Omega Turbulence Models.* [Online]
Available at: https://help.autodesk.com/view/SCDSE/2023/ENU/?guid=GUID-0F5C4828-9F91-46B6-A16A-2578D72DCFCC

[17] Langley Research Center, 2013. *Turbulence Modeling Resource.* [Online]
Available at: https://turbmodels.larc.nasa.gov/sst.html
[Accessed 08 7 2013].

[18] E.C.Maskell, 1963. *A theory of the blockage effects on bluff bodies and stalled wings in a closed wind tunnel.* London, Her majesty's stationery Office.

[19] R.Fail, J.A.Lawford & R.C.W.Eyre, 1959. *Low-Speed-Experiments. on the Wake Characteristics of Flat Plates normal to an Air Stream.* London, HER MAJESTY'S STATIONERY OFFICE .

[20] Frank, M. W., 2011. *Fluid Mechanics.* 8 ed. New York: McGraw-Hill Education.